cmgh
CELLULAR AND MOLECULAR GASTROENTEROLOGY AND HEPATOLOGY

ORIGINAL RESEARCH

Loss of SPTBN1 Suppresses Autophagy Via SETD7-mediated YAP Methylation in Hepatocellular Carcinoma Initiation and Development

Shuyi Chen,[1,*] Huijie Wu,[1,*] Zhengyang Wang,[1] Mengping Jia,[1] Jieyu Guo,[1] Jiayu Jin,[1] Xiaobo Li,[1] Dan Meng,[1] Ling Lin,[2] Aiwu Ruth He,[2] Ping Zhou,[1] and Xiuling Zhi[1]

[1]Department of Physiology and Pathophysiology, School of Basic Medical Sciences, Fudan University, Shanghai, China; [2]Department of Medicine and Oncology, Lombardi Comprehensive Cancer Center, Georgetown University, Washington, DC, USA

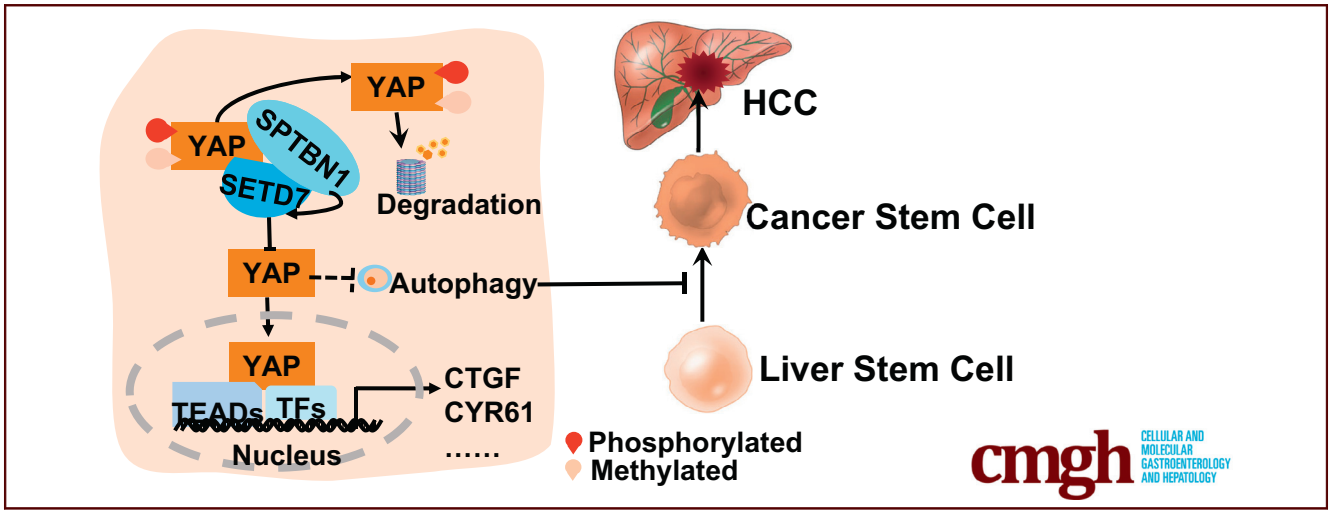

SUMMARY

Spectrin beta, non-erythrocytic 1 cooperates with suppressor of variegation 3-9-enhancer of zeste-trithorax domain containing lysine methyltransferase 7 to promote Yes-associated protein methylation, enhancing autophagy of hepatic stem cells, hepatocellular carcinoma cells, and hepatocytes. Loss of spectrin beta, non-erythrocytic 1 promotes expansion and malignant transformation of hepatic stem cells via inhibiting autophagy during hepatocarcinogenesis.

BACKGROUND & AIMS: Loss of Spectrin beta, non-erythrocytic 1 (SPTBN1) plays an important role in the carcinogenesis of hepatocellular carcinoma (HCC); however, the mechanisms underlying its involvement remain poorly understood. Defects in autophagy contribute to hepatic tumor formation. Hence, in this study, we explored the role and mechanism of SPTBN1 in the autophagy of hepatic stem cells (HSCs) and HCC cells.

METHODS: Expansion, autophagy, and malignant transformation of HSCs were detected in the injured liver of *Sptbn1*$^{+/-}$ mice induced by 3,5-diethoxycarbonyl-1,4-dihydrocollidine treatment. Hippo pathway and Yes-associated protein (YAP) stabilization were examined in isolated HSCs, Huh-7, and PLC/PRF/5 HCC cells and hepatocytes with or without loss of SPTBN1.

RESULTS: We found that heterozygous SPTBN1 knockout accelerated liver tumor development with 3,5-diethoxycarbonyl-1,4-dihydrocollidine induction. Rapamycin promoted autophagy in murine HSCs and reversed the increased malignant transformation induced by heterozygous SPTBN1 deletion. Loss of SPTBN1 also decreased autophagy and increased YAP stability and nuclear localization in human HCC cells and tissues, whereas YAP inhibition attenuated the effects of SPTBN1 deficiency on autophagy. Finally, we found that SPTBN1 positively regulated the expression of suppressor of variegation 3-9-enhancer of zeste-trithorax domain containing lysine methyltransferase 7 to promote YAP methylation, which may lead to YAP degradation and inactivation.

CONCLUSIONS: Our findings provide the first demonstration that loss of SPTBN1 impairs autophagy of HSCs to promote expansion and malignant transformation during hepatocarcinogenesis. SPTBN1 also cooperates with suppressor of variegation 3-9-enhancer of zeste-trithorax domain containing lysine methyltransferase 7 to inactive YAP, resulting in enhanced autophagy of HCC cells. These results may open new avenues targeting SPTBN1 for the prevention and treatment of

HCC. *(Cell Mol Gastroenterol Hepatol 2022;13:949–973; https://doi.org/10.1016/j.jcmgh.2021.10.012)*

Keywords: Autophagy; Hepatic Stem Cells; Hepatocellular Carcinoma; SPTBN1; YAP Methylation.

Hepatocellular carcinoma (HCC) seriously threatens patient health, with incidence and mortality ranking fourth and second among malignant diseases in China and seventh and fourth among malignancies worldwide, respectively.[1,2] Due to usually being diagnosed at late and advanced stages, HCC conveys poor overall prognosis and a low 5-year survival rate in patients, although great progress in treatment has been achieved in addition to surgical resection, the primary therapeutic strategy for HCC.[3] Hence, it is of great significance to study the underlying mechanisms of HCC initiation and development for its early prevention and treatment.

Spectrin beta, non-erythrocytic 1 (SPTBN1), also known as ELF, βII spectrin or β2SP, is an important cytoskeletal protein belonging to the spectrin protein family that binds to ankyrin-B, ankyrin-G, and E-cadherin and participates in many cell processes, such as intracellular transport, cell diffusion and adhesion, cell polarity, cell cycle, and DNA repair.[4-7] SPTBN1 recruits SMAD proteins to participate in transforming growth factor (TGF)-β signal transduction, activating downstream genes to influence cell growth.[8-10] *Sptbn1*$^{-/-}$ mice die during embryogenesis due to intestinal, liver, and cardiovascular diseases and neurological defects, most of which occur on day E11.5.[11,12] Loss of SPTBN1 is linked to a variety of tumors, including pancreatic cancer, colon cancer, ovarian cancer, and liver cancer.[13] It has been reported that 40% to 70% of *Sptbn1*$^{+/-}$ mice spontaneously develop liver cancer at 15 months of age. Downregulation of SPTBN1 also promotes a stronger malignant and stemness phenotype in PLC/PRF/5 and SNU449 HCC cells[14] and results in cell-cycle disruption with significant increases in cyclin D1, cyclin-dependent kinase 4, and hyperphosphorylated retinoblastoma protein.[15,16] In addition, low expression of SPTBN1 in human HCC suggests that SPTBN1 might represent a new marker for the diagnosis and prognosis of patients.[11,15,17] However, the detailed role of SPTBN1 in the regulation of HCC initiation and development remains poorly understood.

Hepatic stem cells (HSCs) are a group of progenitor cells that have the ability of self-renewal and bidirectional differentiation into mature hepatocytes and bile duct cells, which are usually present in the Hering duct of the hilar duct area, participating in physiological and pathological processes such as liver development, cell renewal and liver repair and regeneration.[18] Of note, gene mutations, such as in *PTEN* and *TP53*, and/or dysregulation of signaling pathways, such as Wnt/β-catenin, Notch, or TGF-β, regulating cell renewal in HSCs can lead to malignant transformation of HSCs and HCC progression,[19] providing a new direction for studying the molecular pathogenesis of liver cancer.

Many findings have demonstrated that inhibition of autophagy can induce hepatocarcinogenesis by activating HSCs. Autophagy is a dynamic process of "self-digestion" in eukaryotic cells, which acts as a "housekeeper" to cleave misfolded proteins.[20,21] It is regulated by serine/threonine protein kinase and a series of autophagy-related genes (ATGs)[22] and is involved in many pathological processes, including neurodegeneration, infectious disease, and cancer. Specific knockout of *Atg7* in mouse hepatocytes promotes the expansion of HSCs and hepatocarcinogenesis.[23] Autophagy can prevent malignant transformation of stem cells by maintaining their homeostasis.[24]

The Hippo signaling pathway may be activated through the kinase cascade reaction primarily formed by mammalian ste20-like kinases 1/2 (MST1/2), NDR family kinases large tumor suppressor 1/2 (LATS1/2), and Yes-associated protein (YAP), exerting its anticancer function in mammals.[25,26] In addition to phosphorylation by LATS1/2, acetylation, methylation, and glycosylation have been found to modify YAP and regulate its activity, which is closely related to autophagy. YAP liver-specific deficiency reversed HCC development induced by *Atg7* knockout in mouse liver.[23] On the other hand, Aurora A kinase improved YAP stability and protein expression by blocking autophagy to promote lung cancer progression.[27] YAP is also degraded via the autophagy lysosome pathway, as shown by observing its colocalization with lysosomes in *Atg7* knockout mouse liver.[23]

It has been suggested that β-spectrin mutation leads to the decrease or loss of Hippo-YAP signal transduction activity, which might be caused by the destruction of the basic actin network.[28] Similarly, Deng et al reported that spectrin mutation caused YAP accumulation in the nucleus and promoted cell proliferation in *Drosophila*,[29] whereas loss of SPTBN1 reduced phosphorylation levels of LATS1 and YAP and promoted the translocation of YAP in the human colon adenocarcinoma cell line Caco-2.[30] These reports indicate that SPTBN1 is likely to be involved in the regulation of the Hippo pathway, but its specific mechanism remains to be examined.

In this study, we explored the effect of SPTBN1 on hepatic cell autophagy in HCC initiation and development. We found that rapamycin (RAPA) promoted autophagy in

***Authors share co-first authorship.**

Abbreviations used in this article: **ATGs, autophagy-related genes; CH, chromatin; CHX, cycloheximide; CK19, cytokeratin 19; CTGF, connective tissue growth factor; CSC, cancer stem cells; CYR61, cysteine-rich 61; DDC, 3,5-diethoxycarbonyl-1,4-dihydrocollidine; EMT, epithelial-mesenchymal transition; EPCAM, epithelial cell adhesion molecule; FBS, fetal bovine serum; H&E, hematoxylin and eosin; HBSS, Hanks' balanced salt solution; HCC, hepatocellular carcinoma; HSCs, hepatic stem cells; IP, immunoprecipitant; K-M, Kaplan-Meier; LATS1/2, NDR family kinases large tumor suppressor 1/2; LV, lentivirus; MEF, mouse embryonic fibroblast; Me-YAP, YAP methylation; MST1/2, mammalian Ste20-like kinases 1/2; OS, overall survival; qRT-PCR, quantitative real-time-polymerase chain reaction; RAPA, rapamycin; SETD7, suppressor of variegation 3-9-enhancer of zeste-trithorax domain containing lysine methyltransferase 7; siRNA, small interfering RNAs; SPTBN1, Spectrin beta, non-erythrocytic 1; TGF, transforming growth factor; WT, wild-type; YAP, Yes-associated protein.**

Most current article

2352-345X
https://doi.org/10.1016/j.jcmgh.2021.10.012

murine HSCs and reversed the increased malignant transformation induced by heterozygous SPTBN1 deletion. SPTBN1 also cooperates with suppressor of variegation 3-9-enhancer of zeste-trithorax domain containing lysine methyltransferase 7 (SETD7) to promote methylation of YAP, resulting in YAP inactivation and enhanced autophagy of HCC cells. These findings demonstrate the functional significance of SPTBN1 in HCC, providing new targets for early diagnosis and treatment.

Results

The Kinetics of Carcinogenesis Induced by Sptbn1D/- are Drastically Accelerated by Cotreatment With 3,5 diethoxycarbonyl-1,4-dihydrocollidine

Because 40% to 70% of *Sptbn1*$^{+/-}$ mice spontaneously develop liver cancer at the age of 15 months, we utilized 6- to 8-week-old wild-type (WT) and *Sptbn1*$^{+/-}$ male mice administered a 0.1% 3,5-diethoxycarbonyl-1,4-dihydrocollidine (DDC) supplemental diet to accelerate liver cancer formation. Our results showed that 40% of DDC-induced *Sptbn1*$^{+/-}$ mice developed HCC by the age of 3 months, and 100% developed HCC by the age of 5 months (Figure 1*A-C*). In contrast, no WT mice treated with DDC developed HCC at either 3 or 5 months old.

Generally, development and architecture of liver tissues including the biliary epithelium were normal in *Sptbn1*$^{+/-}$ mice (Figure 1*D*). However, the liver volume of *Sptbn1*$^{+/-}$ mice was enlarged compared with that of WT mice treated with DDC for 1 month (Figure 1*E*). Therefore, we focused on the precancerous stage of HCC caused by loss of SPTBN1 after 1 month of DDC cotreatment.

To determine if the malignant transformation of HSCs could be the origination of HCC induced by loss of SPTBN1, murine HSCs were separated from the liver of *Sptbn1*$^{+/-}$ and WT mice (Figure 1*F*). The cultured HSCs showed about 32% epithelial cell adhesion molecule (EPCAM)-positive cell portion (Figure 1*G*). Stem markers were only detected in HSCs, compared with hepatocytes (Figure 1*H*). The expansion and malignant transformation of murine HSCs were evaluated during HCC development in *Sptbn1*$^{+/-}$ mice. As Figure 1*I* and 1*J* show, the mRNA and protein levels of EPCAM, a marker of liver progenitors, were elevated in the isolated and cultured *Sptbn1*$^{+/-}$ HSCs (Figure 1*I-J*). Meanwhile, EPCAM-positive cells increased and extended from the hilar duct area, indicating that HSCs expansion had occurred in DDC-induced *Sptbn1*$^{+/-}$ mouse livers (Figure 1*K*).

Epithelial-mesenchymal transition (EMT) is involved in carcinogenesis and conveys metastatic properties on cancer cells, such as enhanced mobility and invasion and stemness maintenance in tumor stem cells.[31-33] It was reported that EMT was induced by SPTBN1 knockdown in HCC cell lines, as well as in HSCs from interleukin-6-induced *Sptbn1*$^{+/-}$ mice.[14,17] To investigate whether enhanced EMT occurred in HSCs from DDC-induced *Sptbn1*$^{+/-}$ mice, mRNA and protein levels of EMT-related markers were assessed. We found that CDH1/E-cadherin, TJP1/ZO-1, and CLDN1/Claudin-1 expression decreased, and CDH2/N-cadherin, VIM/Vimentin, SNAIL1, SNAIL2, and TWIST1 expression increased (Figure 2*A-B*). Immunofluorescence staining of liver tissue showed that the number of double-positive cells of VIM and cytokeratin 19 (CK19) or EPCAM and CK19 in *Sptbn1*$^{+/-}$ mice was greater than in WT mice (Figure 2*C*). Furthermore, expression of the oncogene AFP, an important marker of liver cancer, was increased at the mRNA and protein levels in HSCs from *Sptbn1*$^{+/-}$ mice (Figure 2*A-B*). Our results suggest that SPTBN1 heterozygosity promotes malignant transformation of murine HSCs, ultimately resulting in HCC development.

SPTBN1 Heterozygous Deletion Promotes the Malignant Transformation of Murine HSCs by Inhibiting Autophagy

Many studies have proven that autophagy suppresses HCC progression at the initial stage. It was also reported that hepatocyte-specific knockout of *Atg7* promotes expansion of HSCs and HCC development.[23] To investigate whether SPTBN1 alters autophagy levels in HSCs, expression of autophagy-related genes was examined. We found that mRNA expression of *Becn1* (*Atg6*), *Atg4b*, *Atg5*, *Atg7*, and *Atg10* was decreased in HSCs from *Sptbn1*$^{+/-}$ mice (Figure 3*A*), whereas *Becn1*, *Atg4b*, and *Atg10* were decreased in *Sptbn1*$^{-/-}$ mouse embryonic fibroblast (MEF) cells (Figure 3*B-C*). Furthermore, the protein LC3B-II/I ratio and BECN1/Beclin-1 expression were downregulated in *Sptbn1*$^{+/-}$ HSCs (Figure 3*D*) and *Sptbn1*$^{-/-}$ MEFs (Figure 3*E*), whereas the number of EPCAM/SQSTM1 double-positive cells in the livers of DDC-treated *Sptbn1*$^{+/-}$ mice was higher compared with DDC-treated WT mice (Figure 3*F*). Our data suggest that the level of autophagy was decreased in HSCs and MEFs due to the loss of SPTBN1.

To further investigate whether SPTBN1 regulates the malignant transformation of murine HSCs through autophagy inhibition, the effect of the autophagy inducer RAPA was assessed. As shown in Figure 4*A* and 4*B*, mRNA level of autophagy related gene *Becn1* and *Atg4b* was decreased, with decreased EMT-related gene *Cdh1* and increased *Vim* in *Sptbn1*$^{+/-}$ HSCs, whereas RAPA reversed the effect of SPTBN1 heterozygosity, as well as the ratio LC3B-II/I at protein level. In DCC-treated *Sptbn1*$^{+/-}$ mice, the size and contour of extensive hyperplastic intrahepatic bile duct were irregular, with co-wall and "back-to-back" phenomenon. The bile duct epithelial was dysplasia, characterized by atypical, enlarged, and hyperchromatic nuclei, an increased nuclear/cytoplasmic ratio, and a loss of polarity, representing precancerous lesion incidences only in the *Sptbn1*$^{+/-}$ mice, whereas the morphological differences were rescued by RAPA injection (Figure 4*C*, upper). Immunofluorescence staining showed that the increased number of EPCAM/SQSTM1 and VIM/CK19 double-positive cells in the livers of DDC-treated *Sptbn1*$^{+/-}$ mice were both reduced by RAPA (Figure 4*C*, lower). Our data indicate that loss of SPTBN1 attenuates autophagy of HCSs, leading to malignant transformation, whereas RAPA induced autophagy and rescued the precancerous phenotype induced by loss of SPTBN1.

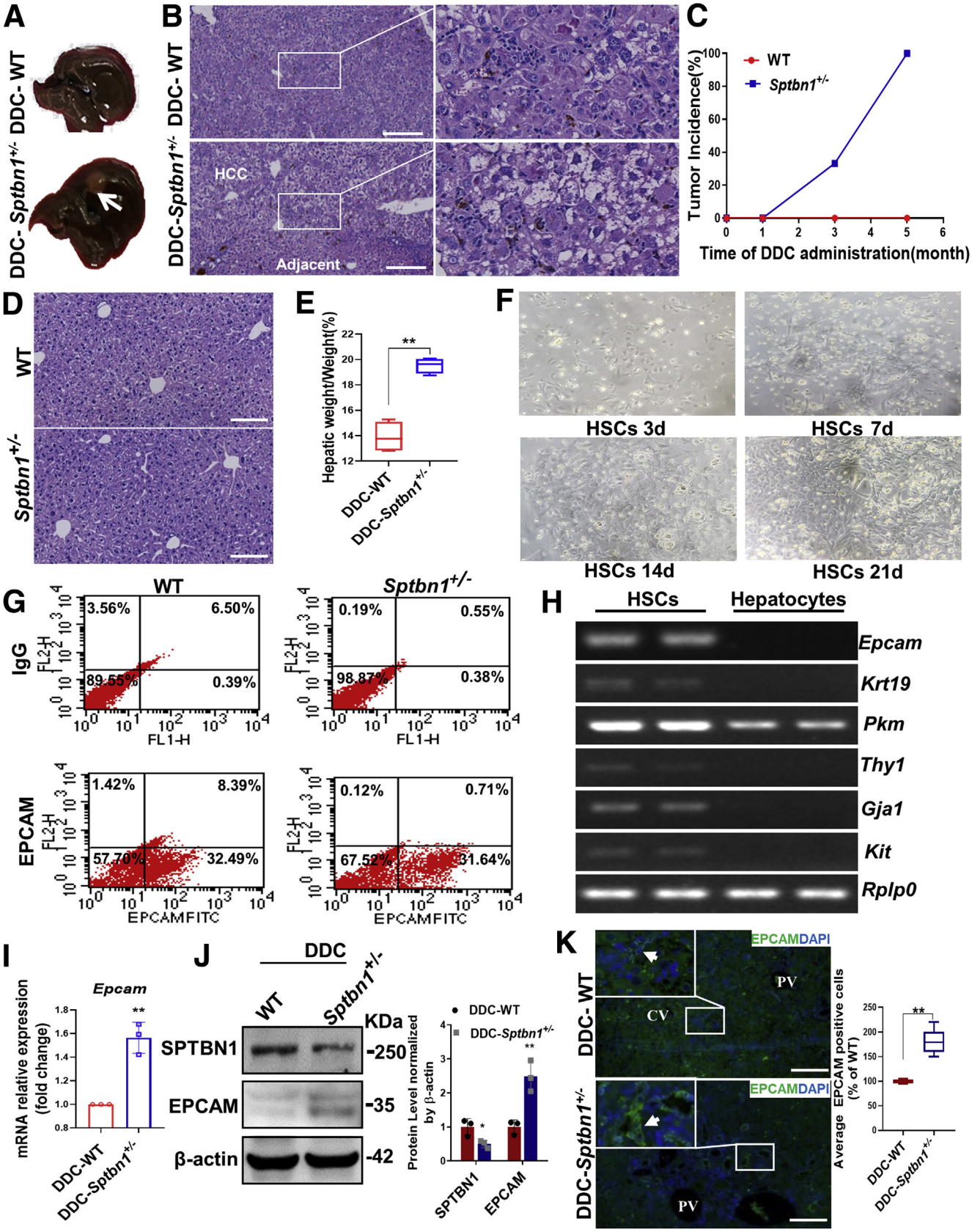
A
DDC- WT
DDC- Sptbn1+/-
B
DDC- WT
DDC-Sptbn1+/-
HCC
Adjacent
C
WT
Sptbn1+/-
Tumor Incidence(%)
Time of DDC administration(month)
D
WT
Sptbn1+/-
E
Hepatic weight/Weight(%)
DDC-WT
DDC-Sptbn1+/-
F
HSCs 3d
HSCs 7d
HSCs 14d
HSCs 21d
G
WT
Sptbn1+/-
IgG
EPCAM
3.56%
6.50%
89.55%
0.39%
0.19%
0.55%
98.87%
0.38%
1.42%
8.39%
57.70%
32.49%
0.12%
0.71%
67.52%
31.64%
FL1-H
EPCAMFITC
H
HSCs
Hepatocytes
Epcam
Krt19
Pkm
Thy1
Gja1
Kit
Rplp0
I
Epcam
mRNA relative expression (fold change)
DDC-WT
DDC-Sptbn1+/-
J
DDC
WT
Sptbn1+/-
KDa
SPTBN1
EPCAM
β-actin
-250
-35
-42
Protein Level normalized by β-actin
DDC-WT
DDC-Sptbn1+/-
SPTBN1
EPCAM
K
EPCAMDAPI
DDC- WT
DDC-Sptbn1+/-
PV
CV
Average EPCAM positive cells (% of WT)
DDC-WT
DDC-Sptbn1+/-

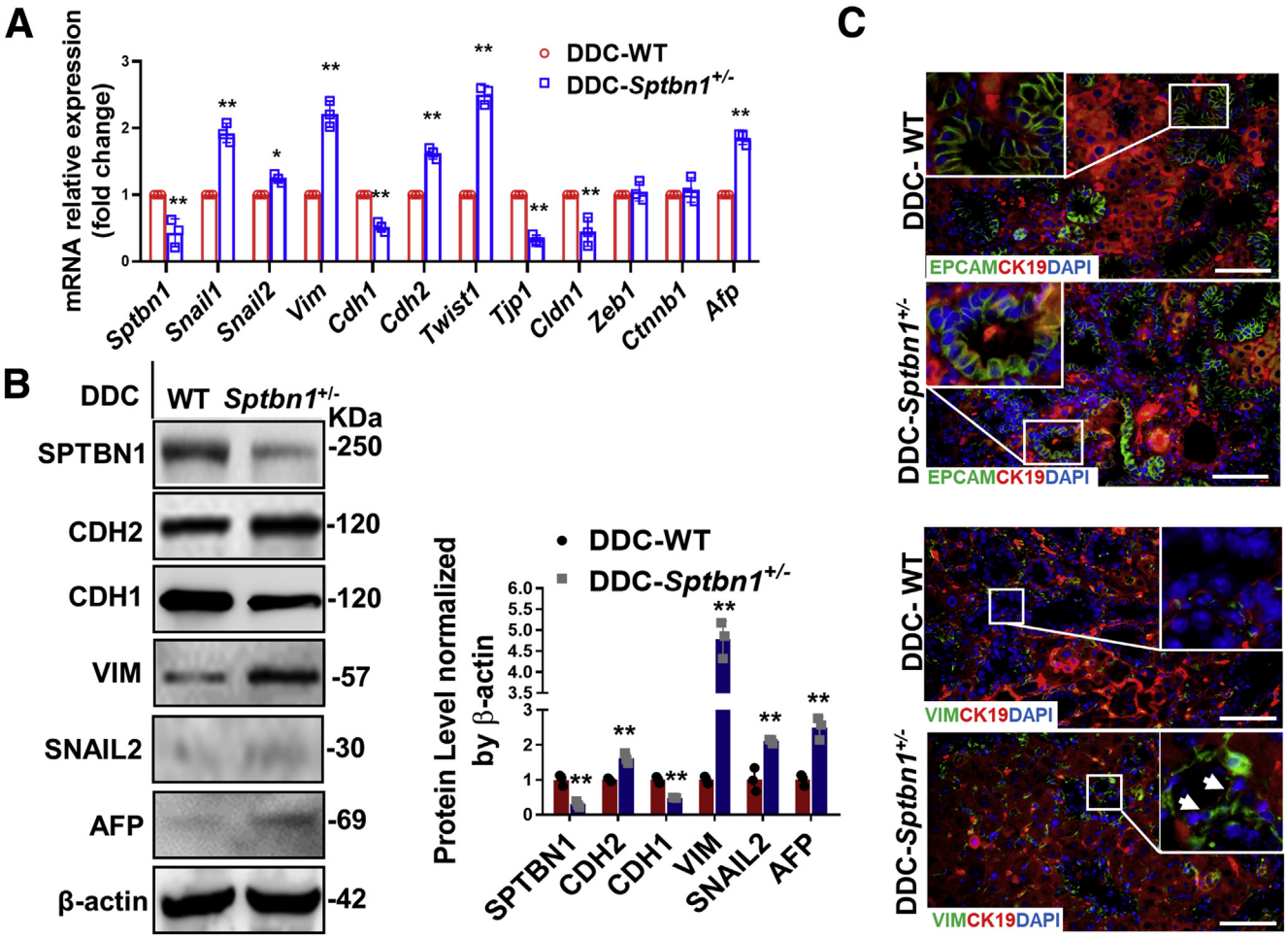

Figure 2. The enhanced EMT occurred in HSCs from DDC-induced *Sptbn1*$^{+/-}$ mice. *A*, QRT-PCR. mRNA levels of *Cdh1*, *Tjp1*, and *Cldn1* were decreased, whereas *Snail1*, *Snail2*, *Vim*, *Cdh2*, and *Twist1* and the tumor marker *Afp* were increased in HSCs from DDC-treated *Sptbn1*$^{+/-}$ mice. *B*, Western blot. Protein levels of CDH1/E-cadherin were decreased, whereas SNAIL2, VIM/Vimentin, CDH2/N-cadherin, and AFP were increased. Data is representative of 3 independent experiments. Significance of the difference was evaluated using the Student *t* test (**P* < .05; ***P* < .01 vs WT). *C*, Immunofluorescence staining. EPCAM/CK19 and VIM/CK19 double-stained cells were increased in the livers of DDC-treated *Sptbn1*$^{+/-}$ mice, and the *arrow* indicates double-stained cells. *White bars* represent 50 μm.

To elucidate the mechanisms of SPTBN1 on HSCs autophagy and HCC development, we performed microarray analysis in EPCAM-positive HSCs from WT and *Sptbn1*$^{+/-}$ mice, and the Kyoto Encyclopedia of Genes and Genomes pathway was utilized with Omicsbean. The Hippo-YAP signaling pathway was one of the identified pathways,

Figure 1. (***See previous page***). **The kinetics of carcinogenesis induced by SPTBN1 heterozygous deletion were accelerated by cotreatment with DDC.** *A*, Liver images of WT and *Sptbn1*$^{+/-}$mice cotreated with DDC. *Arrows* point to HCC in DDC-treated *Sptbn1*$^{+/-}$ mice. Six- to eight-week-old male WT and *Sptbn1*$^{+/-}$ mice (n = 4 for each experiment with 3 experimental replicates) were fed a diet containing 0.1% DDC for 5 months. B, H&E staining of liver sections from WT and *Sptbn1*$^{+/-}$ mice induced by DDC. *White bars* represent 200 μm. *C*, Tumor incidence rate (n = 8). *D*, H&E staining of liver tissues from WT and *Sptbn1*$^{+/-}$ mice aged 6 to 8 weeks. The development and architecture of liver tissues are normal in *Sptbn1*$^{+/-}$ mice. *White bars* represent 100 μm. *E*, The ratio of liver weight to body weight. The liver and body weight of WT and *Sptbn1*$^{+/-}$ mice was measured 1 month after feeding a 0.1% DDC-containing diet (n = 4; ***P* < .01 vs WT). *F*, The morphology of cultured HSCs in 3, 7, 14, and 21 days. *G*, The number of EPCAM-positive cells in HSCs was quantitatively evaluated by flowcytometric analysis. *H*, The stemness nature of cultured HSCs were examined by RT-PCR following by DNA gel electrophoresis. *I-J*, mRNA and protein levels of EPCAM in HSCs of *Sptbn1*$^{+/-}$ mice detected by qRT-PCR (*I*) and Western blot (*J*). Data is representative of 3 independent experiments. Significance of the difference was evaluated using the Student *t* test (**P* < .05; ***P* < .01 vs WT). *K*, Immunofluorescence staining. SPTBN1 heterozygous deletion enhanced expansion of EPCAM-positive (*arrow*) HSCs in DDC-treated livers. CV, Central veins; PV, portal veins. *White bars* represent 100 μm. Number of EPCAM positive cells were counted (n = 4, mean ± standard deviation). Significance of the difference was evaluated using the Student *t* test (***P* < .01 vs WT).

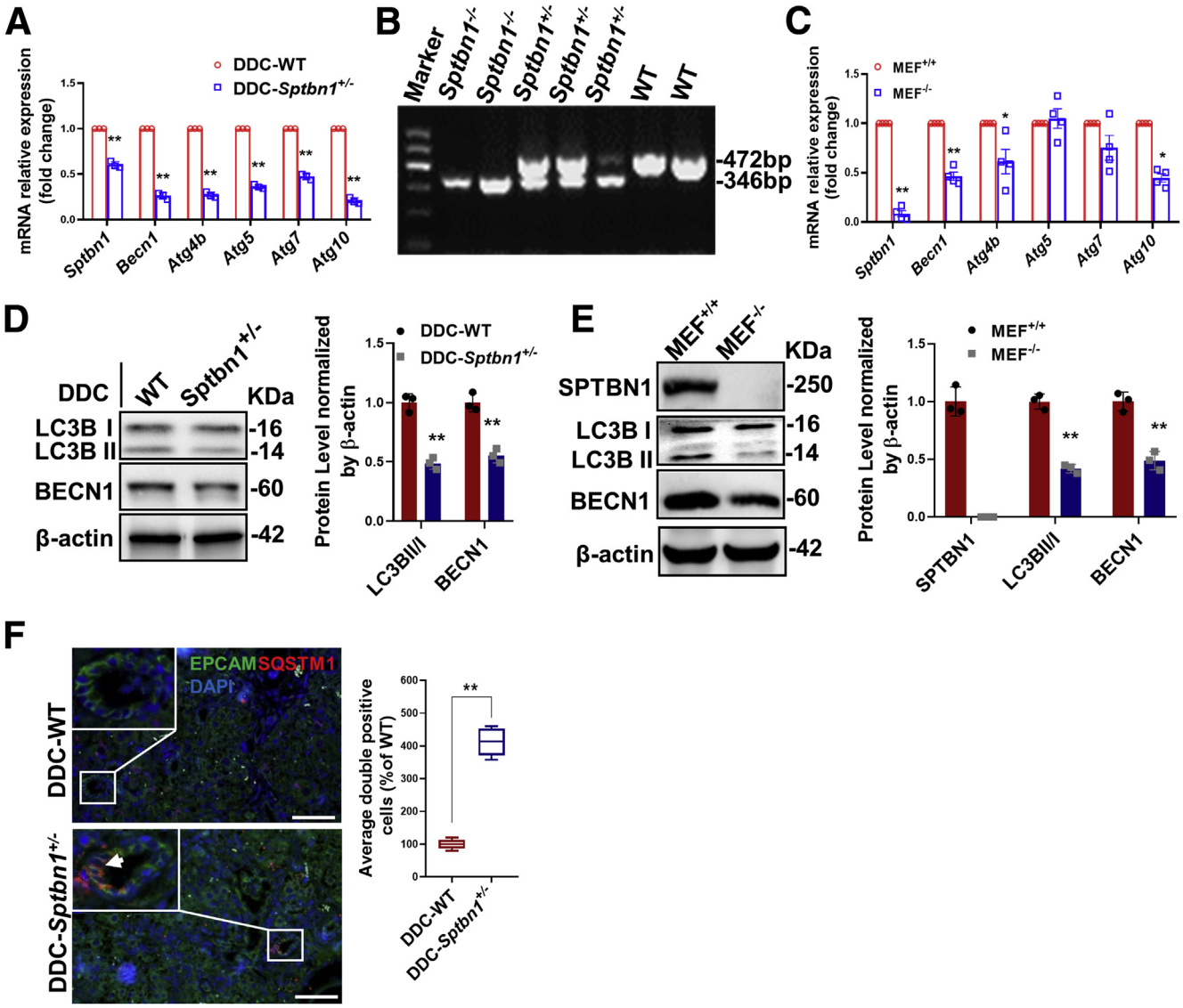

Figure 3. Decreased autophagy level in the *Sptbn1*$^{+/-}$ HSCs and *Sptbn1*$^{-/-}$MEF (MEF$^{-/-}$) cells. *A*, QRT-PCR. mRNA levels of autophagy-related genes *Becn1*, *Atg4b*, *Atg5*, *Atg7*, and *Atg10* were detected by qRT-PCR in HSCs from DDC-treated *Sptbn1*$^{+/-}$ mice. Data is representative of 3 independent experiments. Significance of the difference was evaluated using the Student *t* test (**$P < .01$ vs WT). *B*, Gel electrophoresis of genomic DNA PCR products. The genotypes of MEF cells were clearly visualized. The sequences of primers were Primer 1: TTCCTTCCAGCACCATTCATGT; Primer 2: GGCAGCTCTACC-TACCTGAGT; Primer 3: GCATCGCATTGTCTGAGTAGGT. *C*, QRT-PCR. The mRNA level of autophagy-related genes *Becn1*, *Atg4b*, *Atg5*, *Atg7*, and *Atg10* was analyzed in the MEF cells (*$P < .05$; **$P < .01$ vs MEF$^{+/+}$). *D*, Western blot. The ratio of LC3B-II/I and BECN1 protein levels were decreased in DDC-treated *Sptbn1*$^{+/-}$ mice (**$P < .01$ vs WT). *E*, Western blot. The ratio of LC3B-II/I and protein level of BECN1 were analyzed in the MEF cells (**$P < .01$ vs MEF$^{+/+}$). *F*, Immunofluorescence staining of EPCAM/SQSTM1. EPCAM/SQSTM1 double-stained cells (*arrow pointed*) were increased in the livers of DDC-treated *Sptbn1*$^{+/-}$ mice. *White bars* represent 50 μm (n = 6, mean ± standard deviation). Significance of the difference was evaluated using the Student *t* test (**$P < .01$ vs WT).

exhibiting 44 differential genes (Figure 4*D* and Supplementary Table 1). We then assessed the Hippo-YAP signaling pathway using Western blotting and immunofluorescence in HSCs, livers and MEFs from WT and *Sptbn1*$^{+/-}$ mice. Our results showed that expression of p-YAP^{S127} and p-LATS1 was decreased, whereas expression of total YAP and LATS1 was increased in HSCs from DDC-treated *Sptbn1*$^{+/-}$ mice (Figure 4*E-F*) and *Sptbn1*$^{-/-}$ MEFs (Figure 4*G*), indicating that loss of SPTBN1 elevates the protein level of YAP and inhibits the Hippo signaling pathway.

SPTBN1 Knockdown Decreases Autophagy Levels in HCC Cells

We further examined malignancy and autophagy levels in HCC cells in response to SPTBN1 knockdown. Expression of the stemness marker NANOG and the oncogene

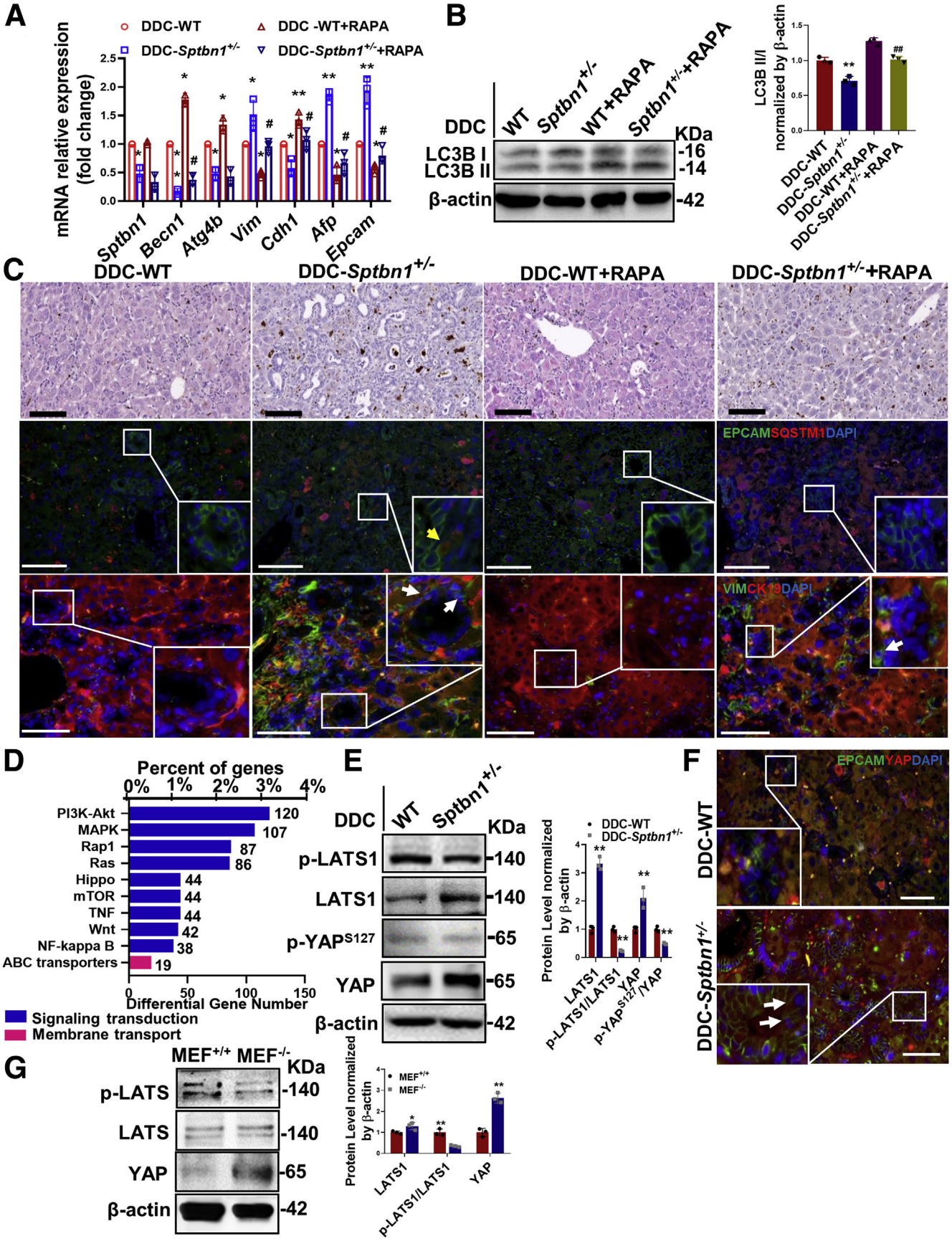
A
DDC-WT
DDC -WT+RAPA
DDC-Sptbn1+/-
DDC-Sptbn1+/-+RAPA
mRNA relative expression (fold change)
Sptbn1
Becn1
Atg4b
Vim
Cdh1
Afp
Epcam
B
DDC
WT
Sptbn1+/-
WT+RAPA
Sptbn1+/-+RAPA
KDa
LC3B I
LC3B II
-16
-14
β-actin
-42
LC3B II/I normalized by β-actin
C
DDC-WT
DDC-Sptbn1+/-
DDC-WT+RAPA
DDC-Sptbn1+/-+RAPA
EPCAMSQSTM1DAPI
VIMCK19DAPI
D
Percent of genes
PI3K-Akt 120
MAPK 107
Rap1 87
Ras 86
Hippo 44
mTOR 44
TNF 44
Wnt 42
NF-kappa B 38
ABC transporters 19
Differential Gene Number
Signaling transduction
Membrane transport
E
p-LATS1
LATS1
p-YAPS127
YAP
Protein Level normalized by β-actin
F
EPCAMYAPDAPI
G
MEF+/+
MEF-/-
p-LATS
LATS
YAP
β-actin

ASCL1 was increased in Huh-7 and PLC/PRF/5 cells transfected with SPTBN1 small interfering RNAs (siRNAs) (Figure 5*A-D*), implying that HCC cells obtained a more malignant phenotype in response to SPTBN1 deficiency. In addition, expression of *BECN1*, *ATG4B*, and *ATG10* at the mRNA level (Figure 6*A*), as well as the LC3B-II/I ratio and expression of BECN1 at the protein level, were significantly reduced in Lentivirus (LV)-SPTBN1-sh stably infected Huh-7 and PLC/PRF/5 cells, whereas protein levels of SQSTM1 were greater in HCC cells (Figure 6*B*) and human HCC tissues with reduced SPTBN1 expression (Figure 6*C-D*), indicating that SPTBN1 knockdown decreased autophagy levels of HCC cells, as well as HSCs. Higher expression of SPTBN1 and lower expression of SQSTM1 were both significantly correlated with increased survival in patients with HCC by performing Kaplan-Meier (K-M) plotter survival analysis (website: http://kmplot.com/analysis/). Interestingly, expression of SPTBN1 was not correlated with prognosis in female patients with HCC (Figure 6*E-H*). Moreover, SPTBN1 overexpression increased autophagy levels of Huh-7 and PLC/PRF/5 cells (Figure 7*A-C*). By electron microscopy, we found that autophagosomes were more enriched in Huh-7 and PLC/PRF/5 cells transfected with CON-sh plasmids than in those transfected with SPTBN1-sh after 24-hour incubation in Hanks' balanced salt solution (HBSS) (Figure 7*D*). To examine the effect of SPTBN1 on the formation of autophagosomes, Huh-7 and PLC/PRF/5 cells with SPTBN1 knockdown were infected with the dual labeled lentivirus GFP-RFP-LC3, which combines an acid-sensitive GFP with an acid-insensitive RFP, monitoring the change from autophagosome (with a neutral pH) to autolysosome (acidic pH). As shown in Figure 7*E*, both autophagosomes and autolysosomes were decreased in response to SPTBN1 knockdown after 24 hours of starvation. Taken together, these data suggest that SPTBN1 knockdown in HCC cells blocks autophagy.

Loss of SPTBN1 Increases Protein Levels and Nuclear Translocation of YAP

As SPTBN1 heterozygosity elevates the protein level of YAP and inhibits the Hippo signaling pathway in *Sptbn1*$^{+/-}$ HSCs, we further verified the effects of SPTBN1 on the Hippo pathway in human HCC cells. We found that mRNA expression of *YAP* and *LATS1* remained unchanged in response to either SPTBN1 knockdown or overexpression (Figure 8*A-B*). In contrast, protein levels of total YAP and LATS1 were increased, whereas the p-YAP^{S127} and p-LATS1 levels were decreased in LV-SPTBN1-sh stably transfected Huh-7 and PLC/PRF/5 cells (Figure 8*C*), which is quite the contrary to those cells with SPTBN1 overexpression (Figure 8*D*). Moreover, YAP nuclear localization was increased in Huh-7 and PLC/PRF/5 cells without SPTBN1 (Figure 8*E-F*). As a result, knockdown of SPTBN1 promoted mRNA expression of YAP targeted gene Cysteine-rich 61 (*CYR61*) and connective tissue growth factor (*CTGF*) (Figure 9*A*). The facts indicated that downregulation of SPTBN1 promotes YAP activation and inactivates the Hippo pathway. Conversely, nuclear YAP levels were decreased (Figure 9*B*), and YAP nuclear translocation was inhibited (Figure 9*C*) by SPTBN1 overexpression.

Consistent with the inhibition of YAP activity by SPTBN1 in Huh-7 and PLC/PRF/5 cells, human HCC tissues with reduced SPTBN1 expression in Figure 6*C* displayed stronger staining of total YAP and weaker staining of p-YAP^{S127} compared with adjacent normal tissues (Figure 9*D*).

Loss of SPTBN1 Inhibits Autophagy by Activating YAP in HCC Cells

We found that SPTBN1 promoted autophagy and inactivated YAP in HCC cells and tissues. Next, we explored whether SPTBN1-induced autophagy was mediated by YAP inactivation. As shown in Figure 10, siRNA targeting YAP reversed mRNA levels of *BECN1*, *ATG4B* and *ATG10* (Figure 10*A-B*) and the ratio of protein LC3B-II/I (Figure 10*C-D*), which was decreased by SPTBN1 knockdown in Huh-7 and PLC/PRF/5 cells. The YAP inhibitor verteporfin had the same effects as YAP siRNA (Figure 10*E-F*). Notably, SPTBN1 knockdown decreased the number of both autophagosomes and autolysosomes in Huh-7 and PLC/PRF/5 cells after 24 hours of starvation, whereas YAP siRNA abrogated this reduction (Figure 10*G*).

Figure 4. (***See previous page***). **SPTBN1 inhibited malignant transformation by promoting autophagy and the Hippo pathway in murine HSCs.** *A and B*, The effect of RAPA was analyzed by qRT-PCR and Western blot. *A*, The mRNA levels of autophagy-related genes *Becn1* and *Atg4b*, EMT-related genes *Vim* and *Cdh1*, *Afp* and *Epcam* were reversed by RAPA in HSCs from DDC-treated *Sptbn1*$^{+/-}$ mice (n = 3; $^{*}P < .05$, $^{**}P < .01$ vs WT, $^{\#}P < .05$ vs *Sptbn1*$^{+/-}$). *B*, The decreased ratio of LC3B-II/I in HSCs from DDC-treated *Sptbn1*$^{+/-}$ mice was rescued by RAPA (n = 3; $^{**}P < .01$ vs WT, $^{\#\#}P < .01$ vs *Sptbn1*$^{+/-}$). *C*, H&E staining of liver sections and immunofluorescence staining of EPCAM/SQSTM1 and VIM/CK19. *Upper,* H&E staining showed the morphological differences of liver tissues in DCC-treated *Sptbn1*$^{+/-}$mice with or without RAPA injection. *Black bars* represent 100 μm. *Lower*, Immunofluorescence staining of EPCAM/SQSTM1 and VIM/CK19. The number of EPCAM/SQSTM1 double-stained cells (*yellow arrow pointed*) and VIM/CK19 double-stained cells (*white arrow pointed*) was decreased in the livers of RAPA- and DDC-treated *Sptbn1*$^{+/-}$ mice compared with DDC-treated *Sptbn1*$^{+/-}$ mice. *White bars* represent 50 μm. *D*, Kyoto Encyclopedia of Genes and Genomes enrichment analysis of EPCAM^{+} HSCs from WT and *Sptbn1*$^{+/-}$ mice. Forty-four different genes in Hippo-YAP signaling pathway were enriched. *E*, The effect of SPTBN1 on the Hippo-YAP pathway in HSCs was examined by Western blot. Protein levels of LATS1 and YAP were increased, whereas those of p-LATS1 and p-YAP^{S127} were decreased in HSCs from DDC-treated *Sptbn1*$^{+/-}$ mice (n = 3; $^{**}P < .01$ vs WT). F. Immunofluorescence staining of EPCAM/YAP. EPCAM/YAP double-stained cells (*arrow*) were increased in the livers of DDC-treated *Sptbn1*$^{+/-}$ mice. *White bars* represent 50 μm. *G*, Western blot. The protein level of p-LATS1, LATS1, and YAP was analyzed by Western blot in the MEF cells ($^{*}P < .05$, $^{**}P < .01$ vs MEF$^{+/+}$).

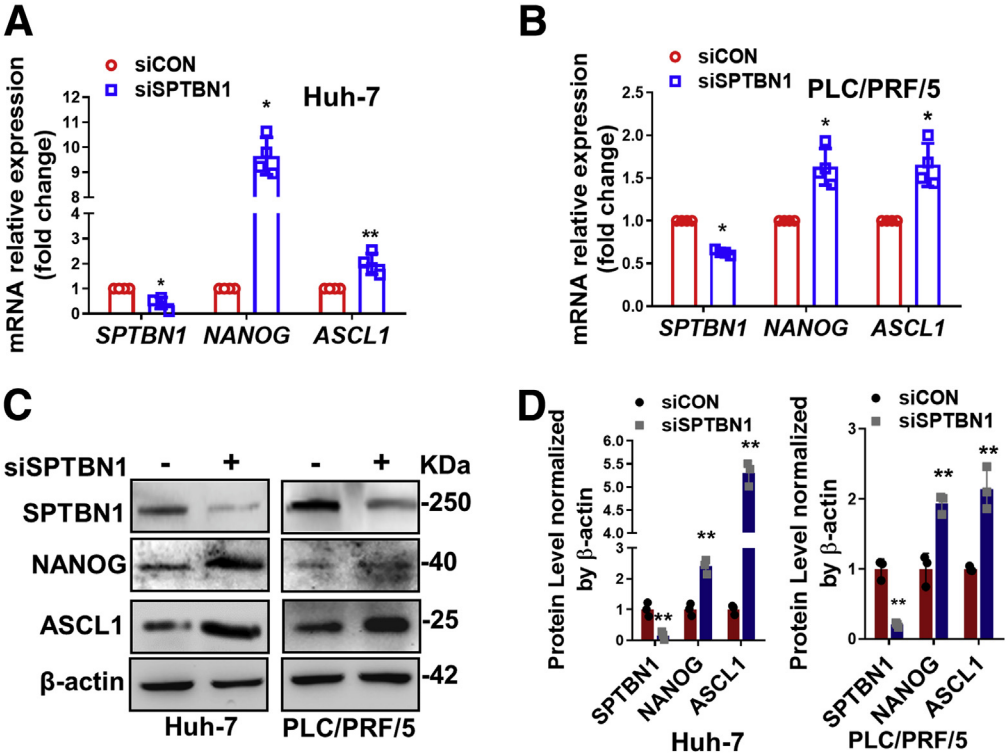

Figure 5. The stemness and malignancy of the HCC cells were increased due to knockdown of SPTBN1. *A and B*, QRT-PCR. The mRNA level of stemness-related marker *NANOG* and oncogene *ASCL1* was increased in the SPTBN1 knockdown Huh-7 (*A*) and PLC/PRF/5 (*B*) cells (n = 4; $^{*}P < .05$, $^{**}P < .01$ vs siCON). *C and D*, Western blot. The protein level of NANOG and ASCL1 was increased in the SPTBN1 knockdown Huh-7 (*C*) and PLC/PRF/5 (*D*) cells ($^{**}P < .01$vs siCON).

SPTBN1 Promotes YAP Degradation and Methylation

Given that SPTBN1 overexpression decreased YAP protein levels, whereas *YAP* mRNA expression was unchanged in Huh-7 and PLC/PRF/5 cells, we reasoned that SPTBN1 would decrease the protein stability of YAP. As shown in Figure 6, blocking proteasome activity with MG132 rescued the decreased levels of YAP induced by SPTBN1 (Figure 11*A*) and enhanced the increase in YAP caused by SPTBN1 knockdown (Figure 11*B*). We also tested the level of p-YAP^{S127} and found that MG132 reversed the decreased ratio of YAP/p-YAP^{S127} induced by SPTBN1 overexpression (Figure 11*A*). Correspondingly, MG132 enhanced the increase of YAP/p-YAP^{S127} caused by SPTBN1 knockdown (Figure 11*B*). Our results demonstrate that loss of SPTBN1 promotes total YAP stabilization by decreasing proteasome degradation. Moreover, besides phosphorylation of YAP, it is possible that other modifications, such as methylation of YAP, may be involved in YAP stabilization induced by loss of SPTBN1.

In the presence of cycloheximide (CHX), an inhibitor of protein translation, SPTBN1 overexpression accelerated the degradation of YAP in Huh-7 cells (Figure 11*C*). This evidence suggests that SPTBN1 promotes YAP degradation through the ubiquitin proteasome degradation system.

As an epigenetic marker, methylation modification of nonhistone proteins can regulate protein stability and nucleoplasm localization.[34] YAP stability is primarily regulated by p-YAP triggered ubiquitination, which eventually leads to YAP degradation under high cell density.[35,36] However, whether methylation-dependent ubiquitination of YAP occurs is currently unknown. We next investigated whether SPTBN1 modulates YAP methylation and promotes YAP ubiquitination and degradation. It was found that methylated YAP protein was increased, whereas expression of total YAP protein was reduced in HCC cells with SPTBN1 overexpression (Figure 11*D-E*), indicating that the reduction in YAP stability caused by SPTBN1 might be related to YAP methylation. In addition, the levels of monomethylation of histone 3 at the lysine 4 site (H3K4me) were increased in response to SPTBN1 overexpression, demonstrating that SPTBN1 also promotes histone methylation.

SPTBN1 Transcriptionally Regulates SETD7 Expression

Next, we performed microarray analysis to identify lysine methyltransferases regulated by SPTBN1. We compared 2 microarrays performed using EPCAM-positive HSCs from WT and *Sptbn1*$^{+/-}$ mice and SNU449 cells with SPTBN1 knockdown and found that expression of the methyltransferase SETD7 was 2.5-fold lower in HSCs and SNU449 cells lacking SPTBN1 (Figure 12*A-B* and Supplementary Table 2). In addition, a positive correlation between SPTBN1 and SETD7 was shown by Gene Expression Profiling Interactive Analysis using HCC retrieved from The Cancer Genome Atlas data (Figure 12*C*). By performing K-M plotter survival analysis (website: http://kmplot.com/analysis/), we observed that higher expression of SETD7 was significantly correlated with increased survival in

patients with HCC (Figure 12*D*). We further verified the correlation between SPTBN1 and SETD7 in Huh-7 and PLC/PRF/5 cells. Quantitative real-time-polymerase chain reaction (qRT-PCR) showed that mRNA levels of *SETD7* were significantly decreased in SPTBN1 siRNA-transfected HCC cells (Figure 12*E*). SPTBN1 knockdown in PLC/PRF/5 cells noticeably inhibited luciferase activity of the *SETD7* promoter but did not decrease luciferase activity of the *SETD7*

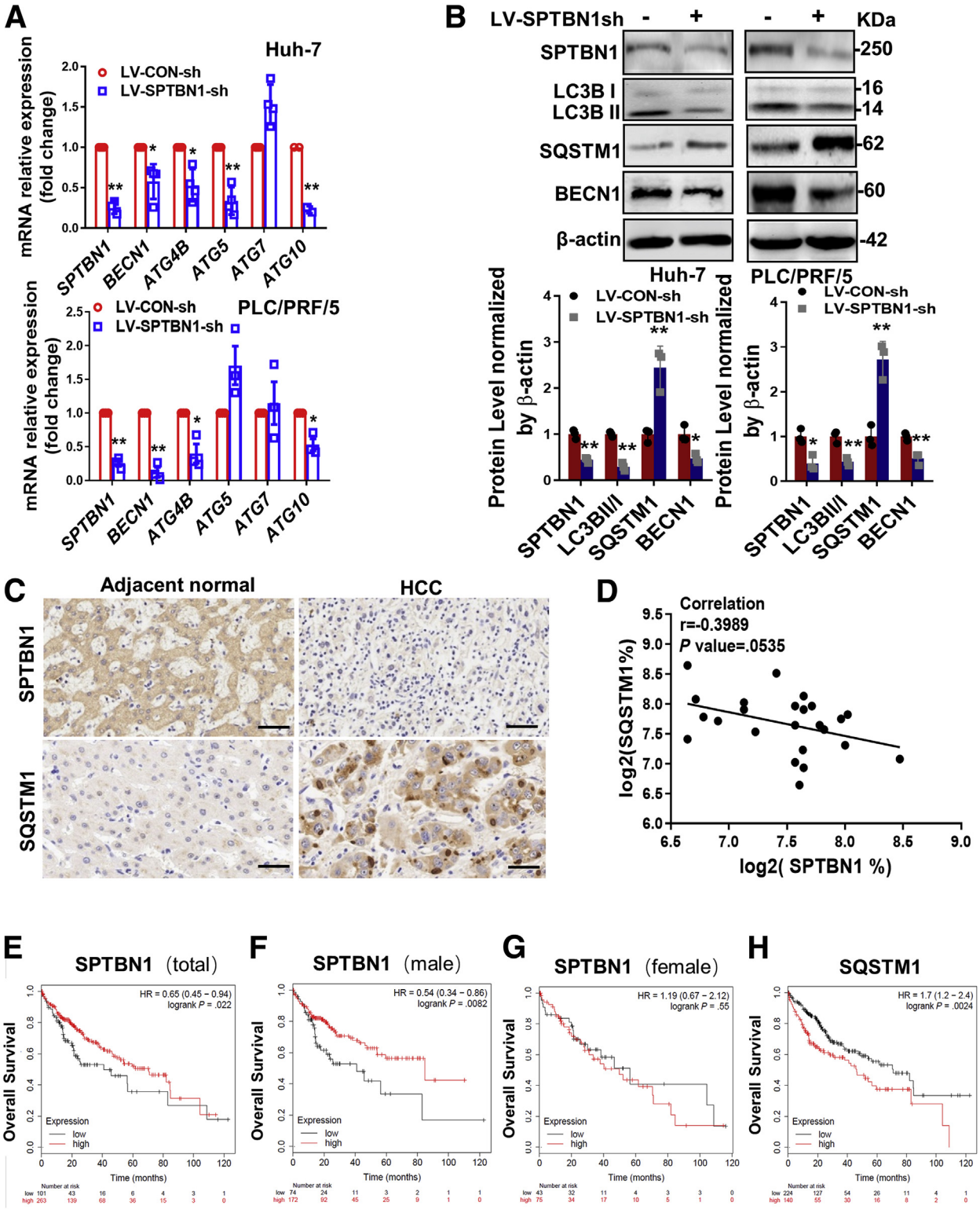

promoter when the SPTBN1 binding site was mutated (Figure 12*F*). In addition, chromatin (Ch)-immunoprecipitant (IP)-PCR showed that SPTBN1 bound to the *SETD7* promoter (Figure 12*G*). Our data demonstrated that SPTBN1 transcriptionally regulates SETD7. Protein levels of SETD7 were also significantly decreased in Huh-7 and PLC/PRF/5 cells in response to SPTBN1 knockdown (Figure 12*H*) but were markedly increased by SPTBN1 overexpression (Figure 12*I*).

YAP Degradation Promoted by SPTBN1 is Mediated by SETD7

The lysine methyltransferase SETD7 is localized both in the cytoplasm and nucleus, modifying histone and nonhistone proteins alike. It has been reported that methylation at lysine (K) 494 of YAP is induced by SETD7, leading to cytoplasmic retention.[37] We previously found that SPTBN1 increases methylation of YAP and promotes degradation of YAP. We further explored whether this effect of SPTBN1 was mediated by SETD7.

We first tested whether SPTBN1 bound to YAP and SETD7. Co-IP assay revealed an interaction between endogenous YAP and SPTBN1, as well as YAP and SETD7, in Huh-7 cells (Figure 13*A*). YAP and SPTBN1, as well as YAP and SETD7, also coprecipitated from the lysate of HEK293 cells engineered to express V5-SPTBN1, Flag-SETD7, and GFP-YAP, suggesting that SPTBN1, SETD7, and YAP combined with one another exogenously (Figure 13*B*).

We next examined whether SETD7 mediated the methylation and degradation of YAP induced by SPTBN1 in PLC/PRF/5 cells. As shown in Figure 13*C*, left, YAP protein levels were increased, whereas YAP methylation (Me-YAP) was decreased, after SPTBN1 knockdown, which was reversed by SETD7 overexpression. Methylation levels of H3K4, a substrate for SETD7, were consistent with Me-YAP.[38] In addition, SETD7 knockdown ameliorated the effect of SPTBN1 overexpression, resulting in greater levels of YAP protein and reduced levels of Me-YAP and H3K4me (Figure 13*C*, right). These findings demonstrate that the methylation and degradation of YAP promoted by SPTBN1 is mediated by SETD7, although the specific mechanisms for the ubiquitination-dependent degradation of YAP require further study.

Loss of SPTBN1 Inhibits Autophagy of Normal Hepatocyte LO2 by Inhibiting YAP Methylation

HCC also possibly originates from differentiated hepatocytes. Therefore, we studied the effect of loss of SPTBN1 on normal hepatocytes using LO2 cell lines. Our results showed that the LC3B-II/I ratio and BECN1 protein level were downregulated; meanwhile SQSTM1 expression was upregulated in LO2 with SPTBN1 knockdown. However, the protein level of EMT-related markers including CDH1, VIM, and SNAIL2 was not changed in LO2 cells after SPTBN1 knockdown (Figure 14*A*). As in HCC cells, *YAP* mRNA expression was unchanged (Figure 14*B*), but the protein level of YAP was increased by SPTBN1 knockdown in LO2 cells (Figure 14*C*), with upregulated mRNA expression of YAP targeted gene *CYR61* and *CTGF* (Figure 14*B*).

Next, we investigated if SPTBN1 modulated SETD7-mediated YAP methylation. Our data showed that the mRNA and protein expression of SETD7 was decreased by SPTBN1 knockdown in LO2 cells as well with decreased Me-YAP, which was reversed by SETD7 overexpression in LO2 cells (Figure 14*B* and *C*, left). SETD7 knockdown ameliorated the effect of SPTBN1 overexpression, resulting in greater levels of YAP protein and reduced levels of Me-YAP (Figure 14*C*, right). Moreover, siRNA targeting YAP reversed the ratio of protein LC3B-II/I, which was decreased by SPTBN1 knockdown in LO2 cells (Figure 14*D*). Comparing the results with those in HSCs, our data suggest that it may be universal that loss of SPTBN1 inhibits autophagy by inhibiting YAP methylation, at least in HCC cell lines, HSCs, and hepatocytes.

Discussion

In addition to the dedifferentiation of mature hepatocytes, accumulating evidence has shown that the abnormal differentiation of HSCs can lead to the development of liver cancer.[19,39] For example, the Hippo-Salvador pathway restrains hepatic oval cell proliferation, liver size, and liver tumorigenesis.[40] Similarly, liver-specific deletion of the neurofibromatosis type 2 tumor suppressor gene in developing or adult mice leads to expansion of stem cells without affecting differentiated hepatocytes; these mice develop HCC and intrahepatic cholangiocarcinoma.[41] Furthermore, any mouse hepatic cells, including hepatic progenitors,

Figure 6. (***See previous page***). **Autophagy levels were decreased in HCC cells and tissues with low SPTBN1 expression.** *A*, QRT-PCR. Huh-7 (*upper*) and PLC/PRF/5 (*lower*) cells infected with LV-CON-sh or LV-SPTBN1-sh were cultured for 72 hours and then subjected to qRT-PCR analysis for *SPTBN1*, *BECN1*, *ATG4B*, *ATG5*, *ATG7*, and *ATG10* mRNA. Data is representative of 3 independent experiments. Significance of the mean value difference was determined using a Student *t* test (*$P < .05$; **$P < .01$ compared with the LV-CON-sh group). *B*, Western blot. The intensities of SPTBN1, LC3B, BECN1, SQSTM1, and β-actin in 3 independent experiments were measured by ImageJ software. Significance of the mean value difference was determined using a Student *t* test (*$P < .05$; **$P < .01$ compared with the LV-CON-sh group). The ratio of LC3BII/LC3BI and protein levels of BECN1 were decreased, whereas SQSTM1 was increased in SPTBN1 knockdown cells. *C*. Immunohistochemistry staining. SPTBN1 and SQSTM1 in and HCC and adjacent noncancerous tissues of patients were stained. *Black bars* represent 50 μm. *D*, Correlation analysis between SPTBN1 and SQSTM1 in patients with HCC by Pearson correlation test ($P = .0535$; $n = 24$). Expression of SPTBN1 in HCC was negatively correlated with SQSTM1, although not significantly. *E, F and G*, The OS was assessed and compared between the low-SPTBN1 and high-SPTBN 1 groups based on extracted clinical data from the The Cancer Genome Atlas in all of 364 patients with HCC (*E*), the 246 male patients with HCC (*F*), and the 118 female patients with HCC (*G*). *H*, The OS was assessed and compared between the low-SQSTM1 and high-SQSTM1 groups.

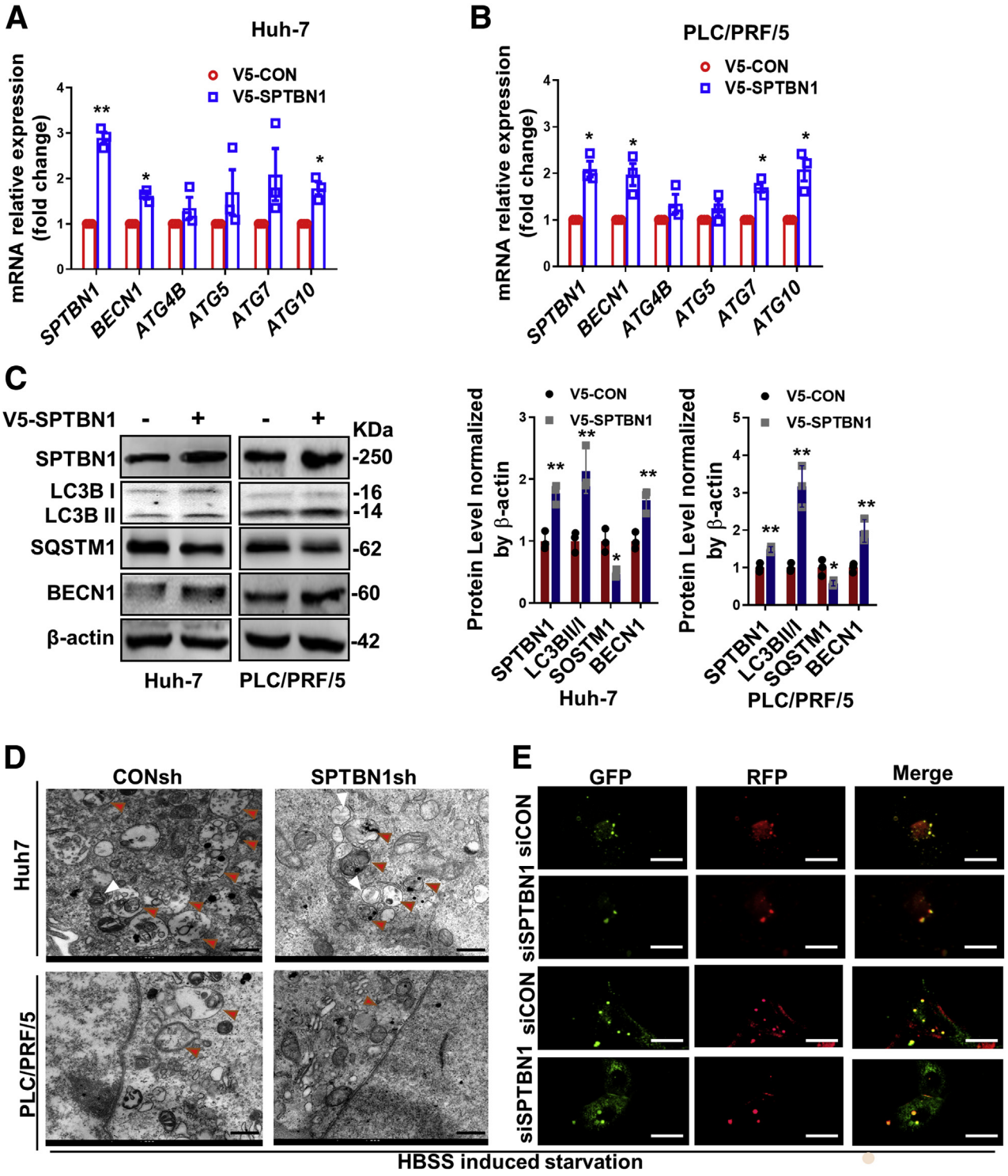

Figure 7. SPTBN1 overexpression increased autophagy level in the HCC cells. *A and B*, QRT-PCR. The mRNA level of autophagy-related genes *BECN1* and *ATG10* was increased in the SPTBN1 overexpression Huh-7 (*A*) and PLC/PRF/5 (*B*) cells. *C*, Western blot. The ratio of LC3BII/LC3BI and the protein level of BECN1 were increased, whereas SQSTM1 was decreased in the SPTBN1 overexpressed Huh-7 and PLC/PRF/5 HCC cells (n = 3; *$P < .05$, **$P < .01$ vs V5-CON). *D*, Transmission electron microscope analysis. Huh-7 (*upper*) and PLC/PRF/5 (*lower*) cells were transfected with CON-sh or SPTBN1-sh plasmids for 48 hours, starved for 24 hours by HBSS, and then examined. Autophagosomes (*white arrow*) and autophagolysosomes (*red arrow*) in HCC cells were reduced in response to SPTBN1 knockdown. *Black bars* represent 500 nm. *E*, Autophagic flux detected by fluorescence microscope. Huh-7 (*upper*) and PLC/PRF/5 (*lower*) cells were infected with GFP-RFP-LC3 LV for 48 hours and then transiently transfected with control siRNA or siRNA to SPTBN1 for another 24 hours. *White bars* represent 10 μm.

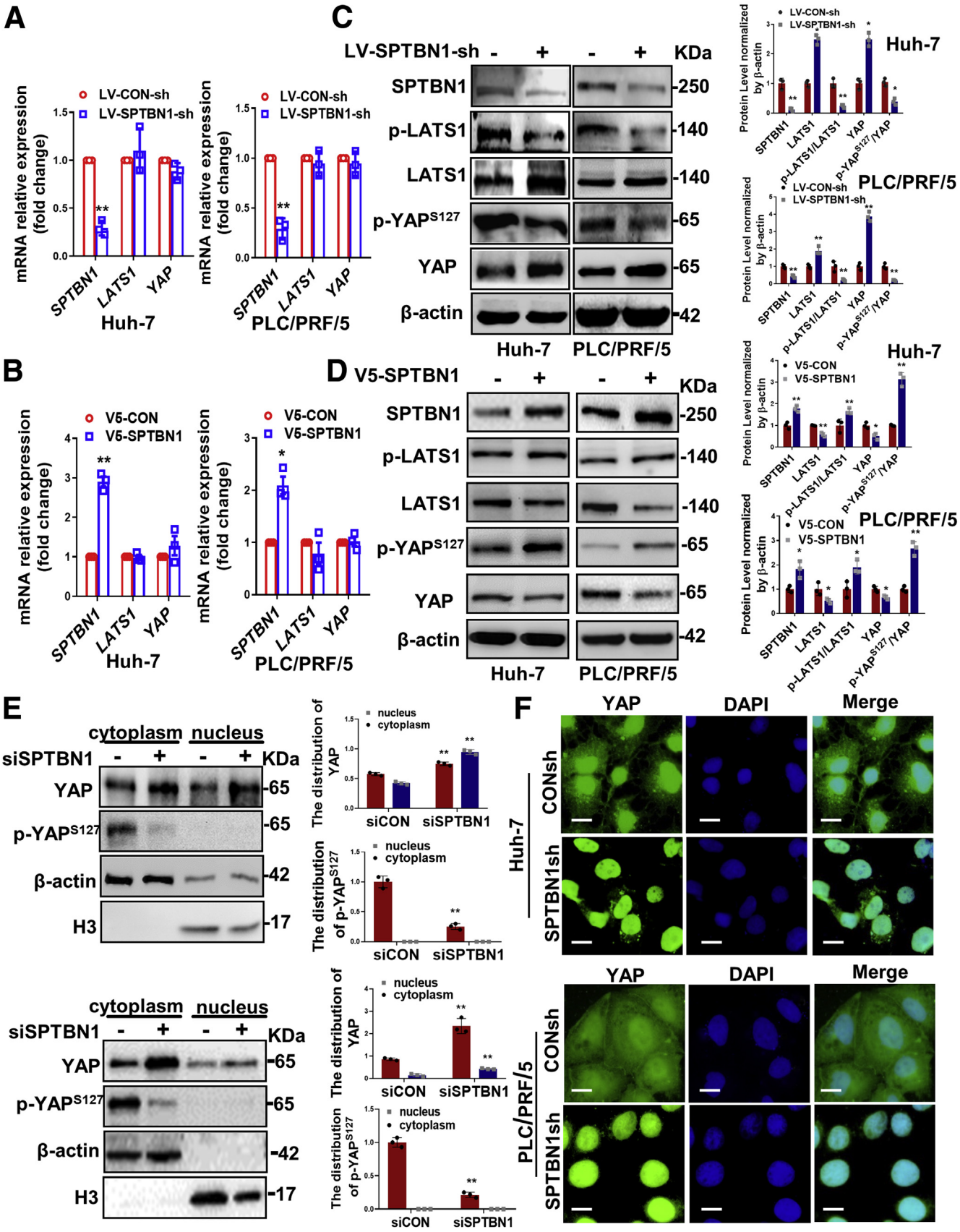
A
LV-CON-sh
LV-SPTBN1-sh
mRNA relative expression (fold change)
SPTBN1
LATS1
YAP
Huh-7
PLC/PRF/5
B
V5-CON
V5-SPTBN1
C
LV-SPTBN1-sh
KDa
SPTBN1
p-LATS1
LATS1
p-YAPS127
YAP
β-actin
Protein Level normalized by β-actin
p-LATS1/LATS1
p-YAPS127/YAP
D
V5-SPTBN1
E
cytoplasm
nucleus
siSPTBN1
H3
The distribution of YAP
The distribution of p-YAPS127
siCON
siSPTBN1
F
YAP
DAPI
Merge
CONsh
SPTBN1sh

hepatoblasts, that express activated oncogenes (such as *H-RAS* or *SV40LT*) can undergo transformation to develop into intrahepatic cholangiocarcinoma or HCC.[42] Dysregulation of liver developmental miRNAs in EPCAM-positive HSCs contribute to liver carcinogenesis by promoting the transformation of HSCs to cancer stem cells (CSCs) of HCC.[43] Ring1 promotes the transformation of HSCs into CSCs, then developing into HCC, through the Wnt/β-catenin signaling pathway.[44] Based on above evidence, HSCs are possibly one of the origins of HCC.

Autophagy is a double-edged sword for HCC that plays different roles during different stages of cancer development. Increasing studies have proven that basal autophagy acts as a tumor suppressor by removing damaged organelles and reactive oxygen species, maintaining genome stability, and preventing malignant transformation of cells.[23] It has been reported that *Becn1*$^{+/-}$ mice spontaneously develop HCC at the age of 18 to 22 months. Hepatocyte-specific knockout of *Atg5* and *Atg7* in mice stimulates hepatomegaly, hepatic adenoma, and even HCC formation.[23] Hence, defects in autophagy promote the occurrence of HCC.

Furthermore, heterozygous deletion of SPTBN1 constitutively activates the NF-κB signaling pathway in the inflammatory environment mediated by interleukin-6, and subsequently, the crosstalk between the activated NF-κB pathway and inactivated TGF-β pathway promote the transformation of HSCs into CSCs, leading to the development of liver cancer.[17] However, it remains unclear if autophagy was involved in loss of SPTBN1-induced malignant transformation of HSCs.

In our study, we demonstrated that EPCAM-positive HSCs expanded in the injured liver of *Sptbn1*$^{+/-}$ mice induced by DDC treatment, also enhancing EMT and increasing expression of the oncogene AFP. Consistent with above reports, our results indicated that HSCs might be reprogrammed into CSCs in the persistent inflammatory microenvironment in the liver of *Sptbn1*$^{+/-}$ mice.[17] Meanwhile, our data confirmed the role of the loss of SPTBN1 in suppressing HSC autophagy both *in vitro* and *in vivo* and that autophagy activation by RAPA blocks the malignant transformation of HSCs caused by SPTBN1 heterozygosity.

The Hippo-YAP signaling pathway plays an important role in regulating stem cell self-renewal, tissue regeneration, and organ size, and its disruption leads to malignant transformation of HSCs and tumor development.[20,45] Knockout of MST1/2, Sav family WW domain-containing protein 1 and neurofibromatosis type 2 (mammalian homolog of Merlin), or overexpression of YAP in mouse liver causes expansion of HSCs or dedifferentiation of hepatocytes, leading to hepatomegaly and hepatocarcinogenesis.[26,40,41,45,46] Moreover, the Hippo-YAP signaling pathway has been reported to regulate autophagy levels. In mammalian cells, MST1/2 promotes autophagy by directly phosphorylating LC3 at threonine 50,[47] whereas silencing of YAP promotes autophagy in glioblastoma and thyroid cancer.[48,49] In our study, we further observed that loss of SPTBN1 contributes to YAP activation *in vitro* and *in vivo*. Downregulation of SPTBN1 in Huh-7 and PLC/PRF/5 cells inhibited autophagy by increasing YAP expression or activity. Lee *et al*[23] also reported that loss of autophagy promotes the expansion of HSCs and hepatocarcinogenesis by inhibiting YAP degradation, whereas deletion of YAP reversed the promoted hepatocarcinogenesis by loss of ATG7. So, we speculate that autophagy and YAP is possibly negatively correlated with each other.

Phosphorylation of YAP has great significance for its nuclear localization and degradation. It was found that YAP has 5 common serine motifs (HXRXXS) that are phosphorylated by LATS1. The phosphorylation sites include S61, S109, S127, S164, and S381. YAP binds to 14-3-3 protein and remains in the cytoplasm after phosphorylation at the S127 site. YAP phosphorylation at the S381 site leads to instability and degradation.[35,36] In addition to the autophagy lysosomal degradation pathway, YAP is primarily degraded through the ubiquitin proteasome pathway by recruiting the E3 ubiquitin ligases SCF$^{\beta\text{-TRCP}}$, FBXW7, and SOCS5/6.[35,50,51] Our results demonstrated that SPTBN1 reduced protein levels of LATS1 and YAP and increased levels of p-LATS1 and p-YAP^{S127}, leading to decreased YAP nuclear localization in Huh-7 and PLC/PRF/5 HCC cells. Furthermore, MG132 enhanced the increase of YAP/p-YAP^{S127} caused by SPTBN1 knockdown, indicating that loss of SPTBN1 promoted total YAP stabilization by decreasing proteasome degradation. In addition, it is possible that other modifications besides phosphorylation of YAP may be involved in YAP stabilization induced by loss of SPTBN1.

SET1A methylates YAP at the K342 site to inhibit YAP binding to CRM1, preventing YAP from exiting the nucleus and promoting tumorigenesis.[52] Another SET domain lysine methyltransferase, SETD7, although classified as an H3K4-specific enzyme, plays a more important role in the

Figure 8. (***See previous page***). **Loss of SPTBN1 increased protein levels and nuclear translocation of YAP. *A and B*, QRT-PCR.** *A*, mRNA levels of *LATS1* and *YAP* were not affected by SPTBN1 knockdown in Huh7 (*left*) or PLC/PRF/5 (*right*) cells (n = 3; $^{**}P < .01$ vs LV-CON-sh). *B*, The mRNA level of *LATS1* and *YAP* was not altered by SPTBN1 overexpression in the Huh-7 and PLC/PRF/5 cells (n = 3; $^{*}P < .05$, $^{**}P < .01$ vs V5-CON). *C and D*, Western blot. *C*, Protein levels of LATS1 and YAP were increased, whereas phosphorylated LATS1 and YAP were decreased in Huh7 (*left*) and PLC/PRF/5 (*right*) cells in response to SPTBN1 knockdown. Significance of the mean value difference was determined using a Student *t* test ($^{*}P < .05$; $^{**}P < .01$ compared with the LV-CON-sh group). *D*, The protein level of LATS1 and YAP was decreased, whereas the phosphorylation of LATS1 and YAP were increased by SPTBN1 overexpression (n = 3; $^{*}P < .05$, $^{**}P < .01$ vs V5-CON). *E*, Huh-7 (*upper*) and PLC/PRF/5 (*lower*) cells were transiently transfected with control siRNA or siRNA to SPTBN1 for 48 hours. Nucleus and cytoplasm proteins were extracted, respectively, for Western blot analysis. Significance of the mean value difference was determined using a Student *t* test ($^{**}P < .01$ compared with the siCON group). *F*, Immunocytofluorescence staining. Loss of SPTBN1 promoted nuclear translocation of YAP in Huh7 (*upper*) and PLC/PRF/5 (*lower*) cells. *White bars* represent 20 μm.

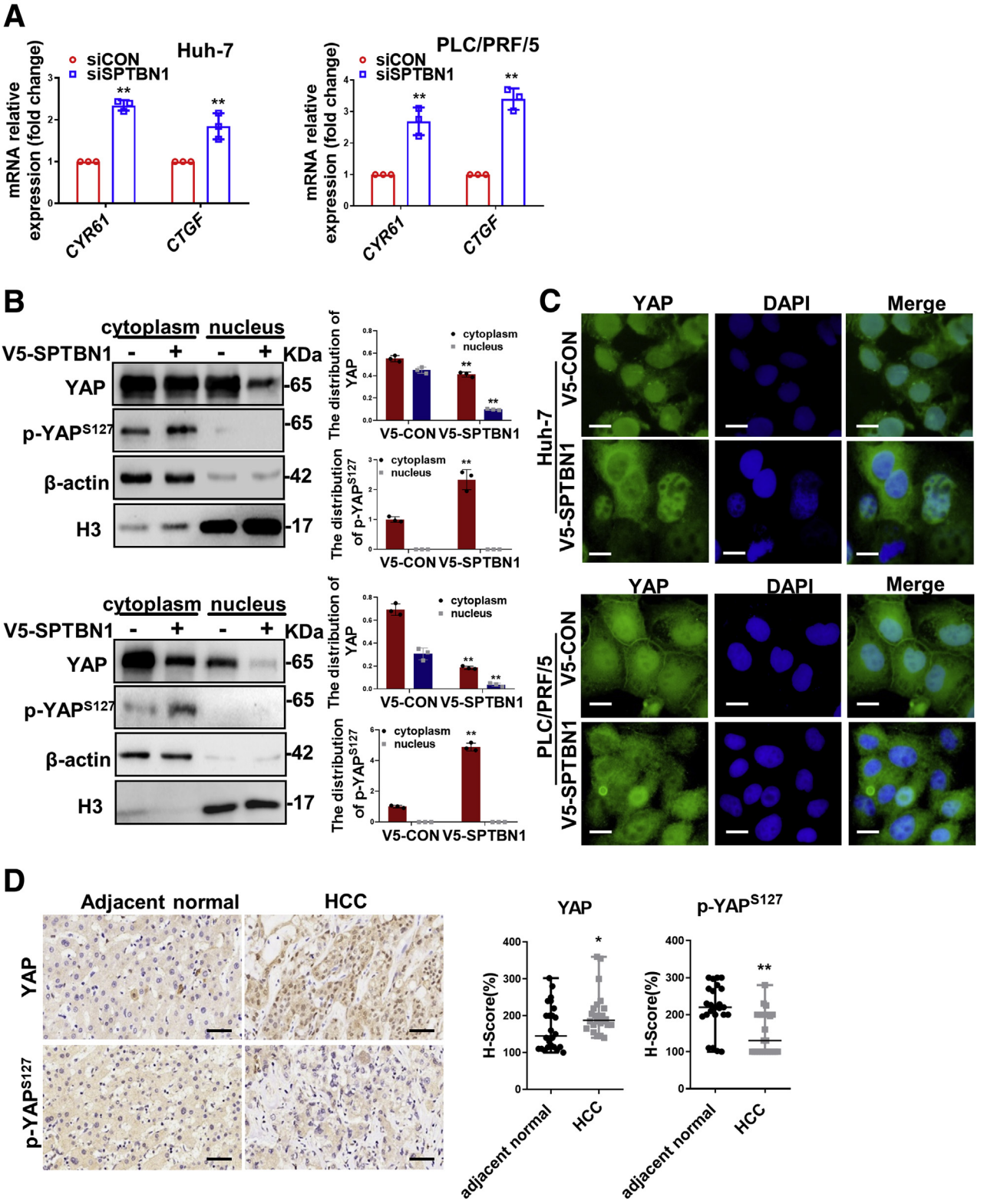

Figure 9. SPTBN1 overexpression inhibited YAP nuclear translocation. *A*, Huh-7 (*left*) and PLC/PRF/5 (*right*) cells were transiently transfected with siRNAs for 48 hours before mRNA levels of *CYR61* and *CTGF*, downstream target genes of YAP, were detected (n = 3; $^{**}P < .01$ vs siCON). *B*, Western blot. The protein levels of YAP were reduced in both the nucleus and cytoplasm, whereas the p-YAP^{S127} level was elevated in the cytoplasm by SPTBN1 overexpression in the Huh-7 (*upper*) and PLC/PRF/5 (*lower*) HCC cells ($^{**}P < .01$ vs V5-CON group). *C*, Immunocytofluorescense staining. YAP was decreased in the nucleus of the Huh-7 (*upper*) and PLC/PRF/5 (*lower*) HCC cells with SPTBN1 overexpression. *White bars* represent 20 μm. *D*, Immunohistochemistry of YAP in human HCC tissues. Expression of total YAP was greater, and p-YAP^{S127} was lower in HCC tissues from patients compared with adjacent noncancerous tissues (*left*) with corresponding statistical results of immunohistochemistry (*right*). *Black bars* represent 50 μm ($^{*}P < .05$, $^{**}P < .01$ compared with adjacent normal).

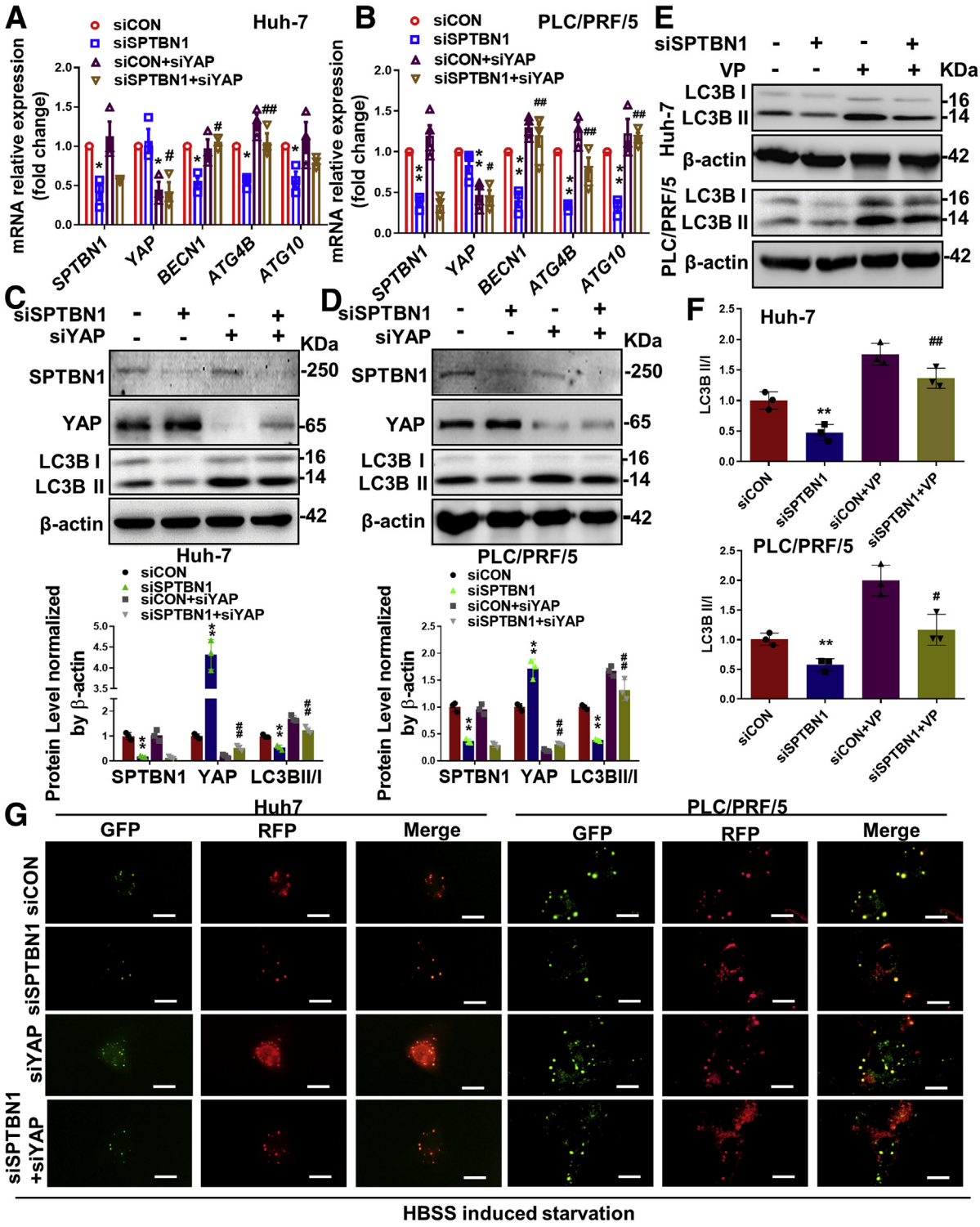

Figure 10. Loss of SPTBN1 inhibited autophagy by activating YAP in HCC cells. *A and B*, QRT-PCR. Huh-7 (*A*) and PLC/PRF/5 (*B*) cells were transiently transfected with siRNA to SPTBN1 or/and YAP for 48 hours and then analyzed. YAP siRNA reversed the expression of autophagy-related genes *BECN1* and *ATG4B* that were downregulated by SPTBN1 knockdown (n = 3; $^{*}P < .05$, $^{**}P < .01$ vs siCON, $^{\#}P < .05$, $^{\#\#}P < .01$ vs siSPTBN1). *C and D*, Western blot. The decreased ratio of LC3BII/ LC3B I protein was reversed by YAP siRNA in Huh-7 (*C*) and PLC/PRF/5 (*D*) cells. Significance of the mean value difference was determined using a Student *t* test ($^{**}P < .01$ vs siCON, $^{\#\#}P < .01$ vs siSPTBN1). *E*, Analysis of autophagy level by Western blot. The decreased ratio of protein LC3BII/ LC3B I was reversed by YAP inhibitor verteporfin in the Huh-7 (*upper*) and PLC/PRF/5 (*lower*) HCC cells. *F*, The statistical analysis of Western blot in Figure *E* (n = 3; $^{**}P < .01$ vs siCON, $^{\#}P < .05$, $^{\#\#}P < .01$ vs siSPTBN1). *G*, Autophagy and autophagic flux detection by fluorescence microscopy after GFP-RFP-LC3 LV transfection and HBSS induction for 24 hours. The reduced autophagy spots in response to SPTBN1 knockdown were reversed by YAP siRNA in Huh-7 (*left*) and PLC/PRF/5 (*right*) cells. *White bars* represent 10 μm.

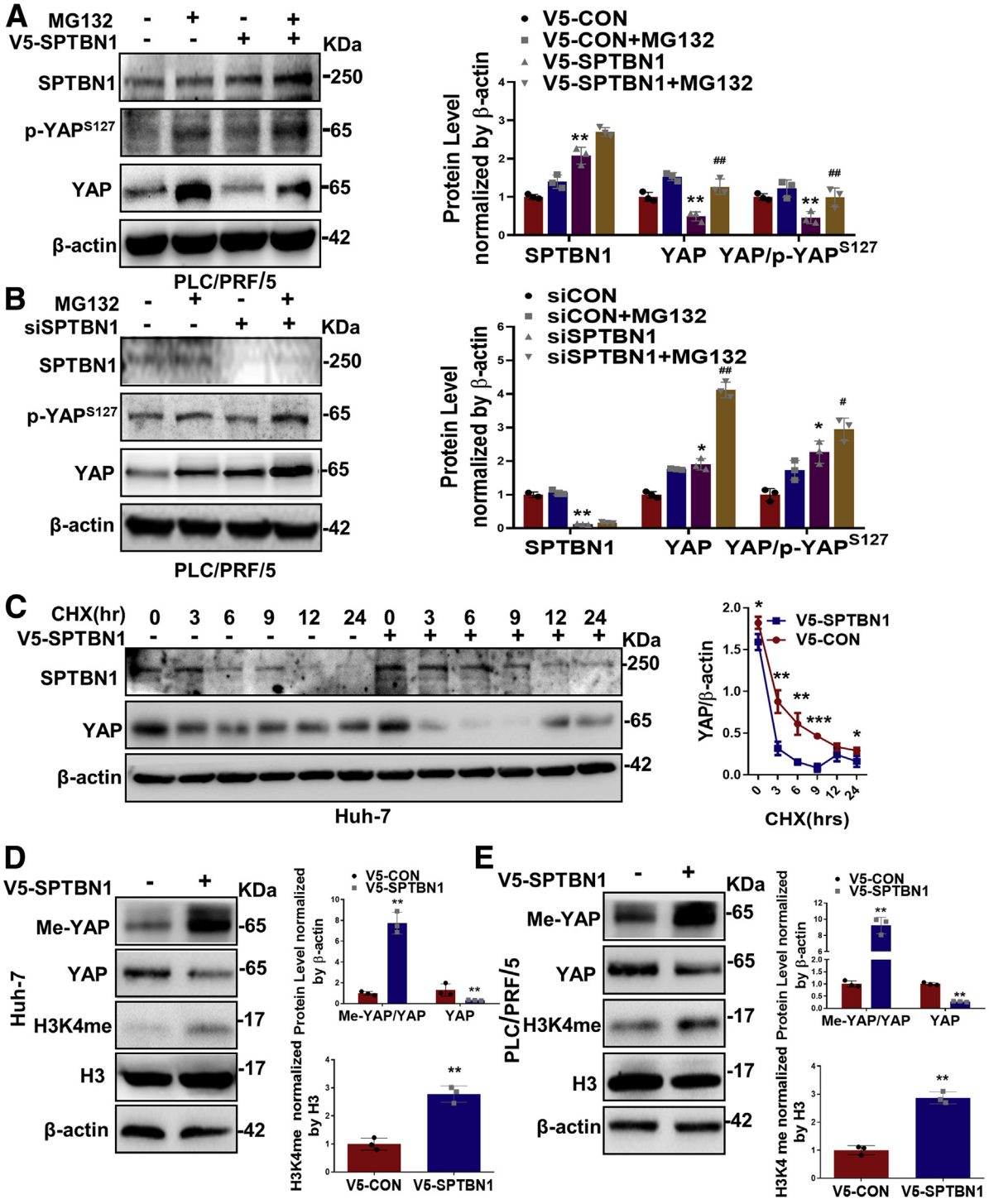

Figure 11. SPTBN1 promoted YAP degradation and methylation. *A and B*, Western blot. For overexpression of SPTBN1 (*A*), PLC/PRF/5 cells were transfected with V5-SPTBN1 plasmid (V5-CON plasmid as blank vector) for 48 hours. For suppression of SPTBN1 (*B*), PLC/PRF/5 cells were transfected with siRNAs to SPTBN1 for 48 hours. Cells then were treated without or with 20 μM MG132 for 3 hours before analyzed by Western blot. The intensities of SPTBN1, YAP, p-YAP^{S127}, and β-actin in 3 independent Western blotting were measured by ImageJ software. *A*, $^{**}P < .01$ vs V5-CON, $^{\#\#}P < .01$ vs V5-SPTBN1. *B*, $^{*}P < .05$, $^{**}P < .01$ vs siCON, $^{\#}P < .05$, $^{\#\#}P < .01$ vs siSPTBN1. *C*, CHX, a protein synthesis inhibitor, was used to detect SPTBN1-regulated YAP stability by Western blot (*left*) in Huh-7 cells. YAP protein had a higher decay rate in cells with SPTBN1 overexpression after CHX pretreatment (*right*) (n = 3; $^{*}P < .05$, $^{**}P < .01$, $^{***}P < .001$ vs V5-CON). *D and E*, The lysis of Huh-7 (*D*) and PLC/PRF/5 (*E*) cells transfected with V5-SPTBN1 plasmids were immunoprecipitated with antibody to YAP, and the immunoprecipitates were then immunoblotted with anti-methylated lysine antibody to detect methylation of endogenous YAP (n = 3; $^{**}P < .01$ vs V5-CON).

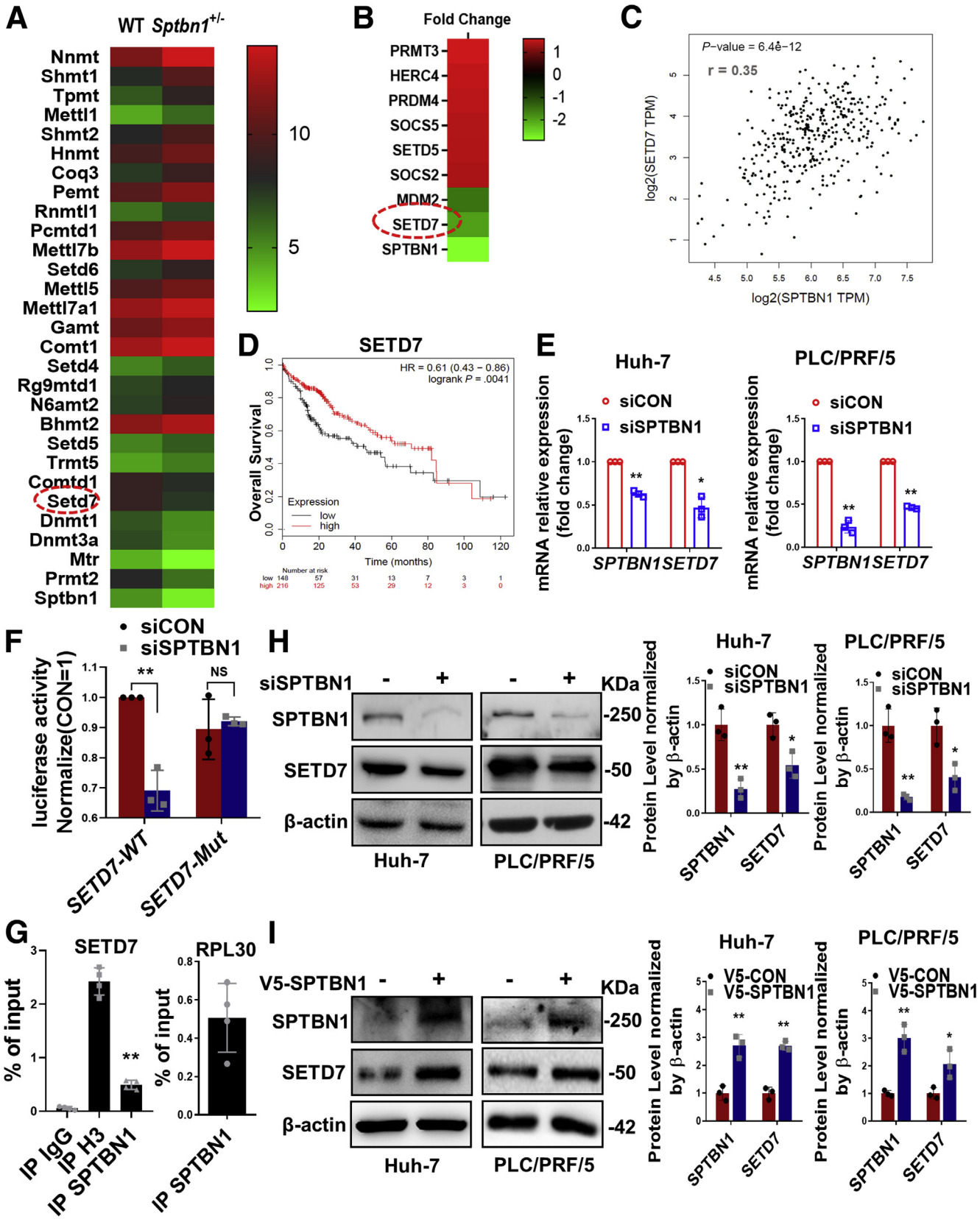
A
WT Sptbn1+/-
Nnmt
Shmt1
Tpmt
Mettl1
Shmt2
Hnmt
Coq3
Pemt
Rnmtl1
Pcmtd1
Mettl7b
Setd6
Mettl5
Mettl7a1
Gamt
Comt1
Setd4
Rg9mtd1
N6amt2
Bhmt2
Setd5
Trmt5
Comtd1
Setd7
Dnmt1
Dnmt3a
Mtr
Prmt2
Sptbn1
10
5
B
Fold Change
PRMT3
HERC4
PRDM4
SOCS5
SETD5
SOCS2
MDM2
SETD7
SPTBN1
1
0
-1
-2
C
P-value = 6.4e-12
r = 0.35
log2(SETD7 TPM)
log2(SPTBN1 TPM)
D
SETD7
HR = 0.61 (0.43 − 0.86)
logrank P = .0041
Overall Survival
Expression
low
high
Time (months)
Number at risk
E
Huh-7
PLC/PRF/5
siCON
siSPTBN1
mRNA relative expression (fold change)
SPTBN1
SETD7
F
siCON
siSPTBN1
luciferase activity Normalize(CON=1)
NS
SETD7-WT
SETD7-Mut
G
SETD7
RPL30
% of input
IP IgG
IP H3
IP SPTBN1
H
siSPTBN1
KDa
SPTBN1
SETD7
β-actin
-250
-50
-42
Huh-7
PLC/PRF/5
Protein Level normalized by β-actin
I
V5-SPTBN1
V5-CON
V5-SPTBN1

cytoplasm. YAP is methylated by SETD7 at K494, causing its retention in the cytoplasm, but the mechanism whereby this occurs is unclear.[38] Our results demonstrated that SPTBN1 enhanced YAP methylation and promoted its degradation by the ubiquitin proteasome pathway in Huh-7 and PLC/PRF/5 cells. Consistent with this observation, SPTBN1 can interact with SETD7 and transcriptionally regulate SETD7 expression. As a result, SETD7 exhibited lower expression in HSCs of *Sptbn1*$^{+/-}$ mice and in HCC cells with suppressed expression of SPTBN1, whereas SETD7 overexpression rescued decreased YAP methylation in response to SPTBN1 knockdown.[38] Our study suggests that YAP activity is regulated not only by the Hippo pathway kinase cascade but also by Hippo-independent mechanisms, such as YAP methylation induction via methyltransferase.

Interestingly, our data suggest that it may be universal that loss of SPTBN1 inhibits autophagy by inhibiting YAP methylation, at least in HCC cell lines, HSCs, and hepatocytes. However, we could not demonstrate malignant transformation of normal hepatocytes *in vitro* by loss of SPTBN1, and it should be studied further whether hepatocytes are another possibility origin of HCC induced by SPTBN1.

In summary, our results suggested that loss of SPTBN1 inhibited HSC autophagy and Hippo pathway and promoted HSC expansion and malignant transformation, leading to hepatocarcinogenesis. SPTBN1 also inhibited autophagy in HCC cells. Loss of SPTBN1 suppresses hepatic cell autophagy via SETD7-mediated YAP methylation, promoting HCC initiation and development. Our study demonstrates new mechanisms of SPTBN1 in inhibiting HCC and provides new targets for HCC treatment.

Methods

Animal Care and Genotyping

SPTBN1 heterozygous (*Sptbn1*$^{+/-}$) mice were generated and amplified as reported[12] by the Shanghai Research Center for Model Organisms (Shanghai, China). Mice were housed in the Experimental Animal Department of Fudan University. All procedures were performed following the approval of the Institutional Animal Care and Use Committee of Fudan University. For mouse genotyping, genomic DNA PCR was employed.

Construction of the *Sptbn1*$^{+/-}$ Liver Injury Model to Induce Activation of HSCs and Liver Cancer

To construct the *Sptbn1*$^{+/-}$ liver injury model, 6- to 8-week-old male WT and *Sptbn1*$^{+/-}$ mice (n = 4, per experiment with 3 experimental replicates) were fed a diet containing 0.1% DDC for 1, 3, and 5 months. At the end of the experiment, mice were weighed and sacrificed to observe liver tumor incidence, and liver tissue was harvested for histological staining.

To elucidate the mechanisms for the malignant transformation of activated HSCs, 6- to 8-week-old male WT and *Sptbn1*$^{+/-}$ mice (n = 4 for each experiment with 3 experimental replicates) were fed a diet containing 0.1% DDC for 1 month and 2 weeks and were injected intraperitoneally with RAPA. In detail, after 2 weeks of treatment with 0.1% DDC, one-half of the paired WT and *Sptbn1*$^{+/-}$ mice were randomly treated with RAPA (2 mg/kg, APExBIO, Houston, TX) by intraperitoneal injection every other day, and the other one-half of the mice were injected with vehicle. One month later, mice were sacrificed, and liver tissues were harvested.

HSC Isolation and Cell Line Culture

Murine HSCs were separated from the liver of *Sptbn1*$^{+/-}$ and WT mice after 1 month of DDC treatment as previously described.[53] In brief, the collected cells were washed and then cultured in Dulbecco's Modified Eagle Medium/F12 medium containing 10% fetal bovine serum (FBS), 20 ng/ml stem cell factor (PeproTech), 10 ng/mL leukemia inhibitory factor (Millipore), 10 ng/mL epidermal growth factor (PeproTech), and 10 ng/mL hepatocyte growth factor (PeproTech). After 7 days, the cells formed a cloned cell cluster. The stemness nature and EPCAM positive

Figure 12. (***See previous page***). **SPTBN1 transcriptionally regulated SETD7 expression.** *A*, Differential expression of methyltransferase in HSCs by microarray analysis. EPCAM-positive HSCs were isolated by flow cytometry from WT and *Sptbn1*$^{+/-}$ mouse livers (n = 3). Then the collected cells were examined by microarray analysis. *B*, Differential expression of methyltransferase in the HCC cells SNU449 by microarray analysis. SNU449 cells were transfected with control siRNA or siRNA to SPTBN1 for 48 hours and screened by microarray analysis. *C*, Correlation analysis between SPTBN1 and SETD7 in patients with HCC was analyzed using The Cancer Genome Atlas database by Gene Expression Profiling Interactive Analysis (r = 0.35; $P < .01$). *D*, The OS was assessed and compared between the low-SETD7 and high-SETD7 groups based on extracted clinical data from The Cancer Genome Atlas in all of 364 patients with HCC. *E*, QRT-PCR. Huh-7 (*left*) and PLC/PRF/5 (*right*) cells were transiently transfected with siRNAs as indicted and then analyzed. Data is representative of 3 independent experiments. Significance of the mean value difference was determined using a Student *t* test (*$P < .05$, **$P < .01$ compared with the siCON group). *F*, Analysis of *SETD7* promoter activity. PLC/PRF/5 cells were transfected with SPTBN1 siRNA or control siRNA for 24 hours and then transfected with a plasmid containing the *SETD7* promoter sequence or a mutated sequence for 24 hours. Then cells were lysed, and luciferase activity was measured (n = 3; **$P < .01$ vs siCON for SETD7-WT group). *G*, ChIP-qPCR. PLC/PRF/5 cells were infected with LV-CON-sh or LV-SPTBN1-sh for 96 hours and then analyzed. IgG antibody was used as a negative control, and H3 antibody was used as a positive control. Homo-RPL30 primers were used as the positive control for ChIP-qPCR detection. *SETD7* promoter region sequences were enriched by SPTBN1 in the obtained ChIP DNA (n = 4; **$P < .01$ vs Ig G). *H*, Western blot. The intensities of SPTBN1, SETD7, and β-actin were measured by ImageJ software, and the ratio of SPTBN1/β-actin and SETD7/β-actin were analyzed by Student *t* test. (*$P < .05$, **$P < .01$ vs siCON, and the data are representative of 3 independent experiments). *I*, Western blot. The protein level of SETD7 was upregulated in the SPTBN1 overexpressed Huh-7 (*left*) and PLC/PRF/5 (*right*) cells (n = 3; *$P < .05$, **$P < .01$ vs V5-CON).

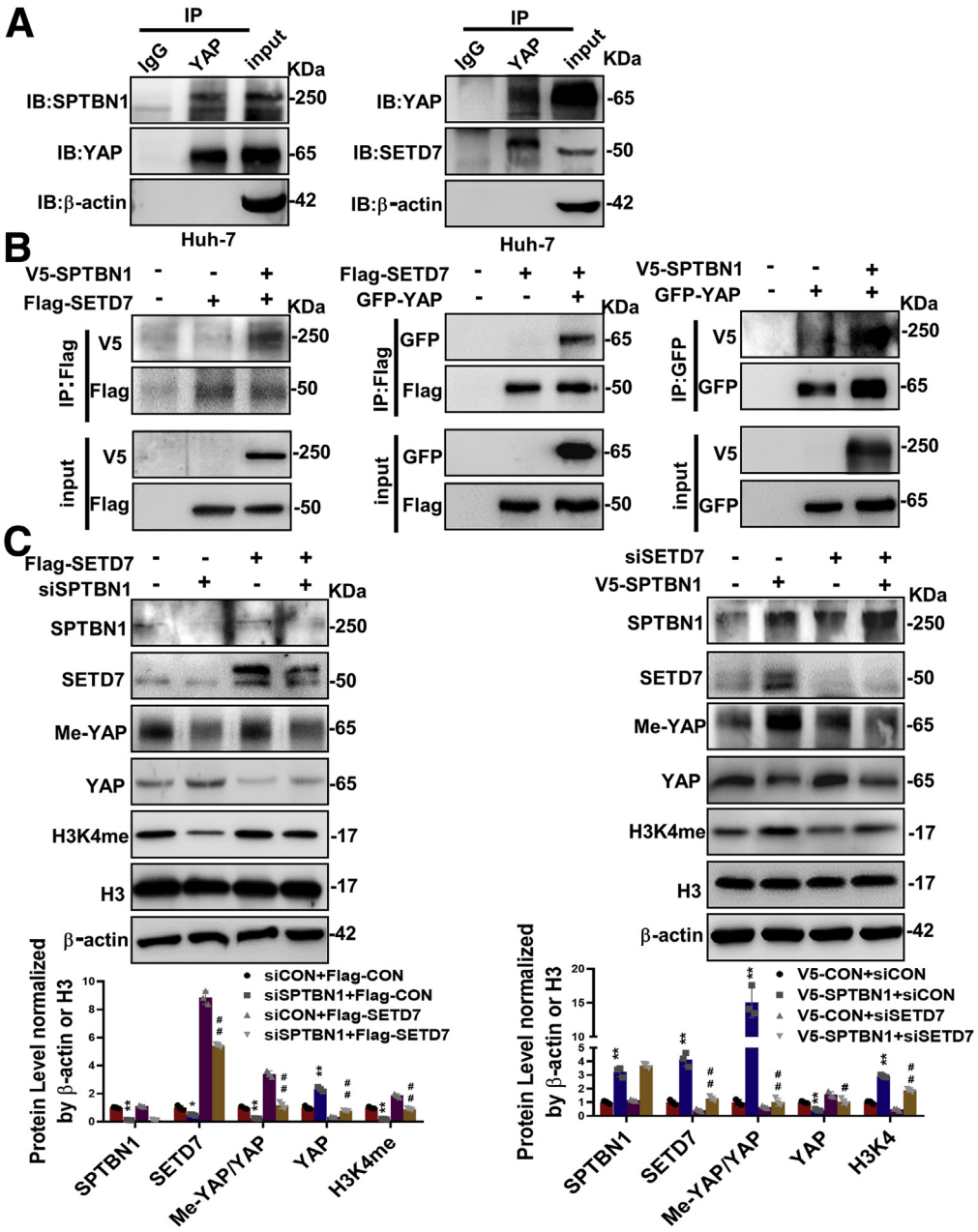

Figure 13. YAP methylation promoted by SPTBN1 was mediated by SETD7. *A and B.* *In vitro* Co-IP experiments. Endogenous YAP was immunoprecipitated from lysates of Huh7 cells (*A*) using a YAP-specific antibody, and Co-IP proteins were analyzed by Western blot using the indicated antibodies. Input: 5% of material used for IP. Lysates from 293 cells (*B*) co-transfected with 2 plasmids of Flag-SETD7, GFP-YAP, and V5-SPTBN1 were immunoprecipitated with an anti-Flag or anti-GFP antibody and then analyzed by Western blot. YAP endogenously interacted with SPTBN1 and SETD7, whereas SPTBN1, SETD7, and YAP interacted exogenously. *C*, Analysis of YAP methylation by Western blot. *Left*, Expression of upregulated YAP and downregulated Me-YAP and H3K4me in PLC/PRF/5 cells with SPTBN1 knockdown was reversed by SETD7 overexpression (*$P < .05$, **$P < .01$ vs siCON, ##$P < .01$ vs siSPTBN1). *Right*, Expression of downregulated YAP and upregulated Me-YAP and H3K4me in SPTBN1-overexpressing PLC/PRF/5 cells was reversed by SETD7 siRNA (**$P < .01$ vs V5-CON, #$P < .05$, ##$P < .01$ vs V5-SPTBN1).

populations of HSCs fractions were examined by RT-PCR and flowcytometric analysis.

The human HCC cell lines Huh-7 and PLC/PRF/5 and normal hepatocytes LO2 were cultured with Dulbecco's Modified Eagle Medium supplemented with 10% FBS and antibiotics. Human embryonic kidney (HEK293T) cells were maintained in Roswell Park Memorial Institute 1640/10% FBS with antibiotics. All cells were cultured in a humidified atmosphere with 5% CO2 at 37°C.

Plasmid and Small Interfering RNA Transfection

For silencing or overexpression of target genes, SPTBN1-sh, V5-SPTBN1, Flag-SETD7, and GFP-YAP were transiently transfected into cells using jetPRIME transfection reagent according to the manufacturer's instructions (Polyplus Transfection SA, France). The siRNAs listed in Supplementary Table 3 were designed and chemically synthesized by GenePharma (Shanghai, China). Cells were also treated with the YAP inhibitor verteporfin (10 μM, APExBIO, Houston, TX) after SPTBN1 siRNA transfection. In one set of experiments in the study, Huh-7 and PLC/PRF/5 cells were infected with LV-SPTBN1-sh purchased from Shanghai Genechem (Shanghai, China). Seventy-two hours after infection, stably transduced cells were selected.

To assess autophagic flux, cells were transfected with SPTBN1 siRNA for 72 hours and then infected with GFP-

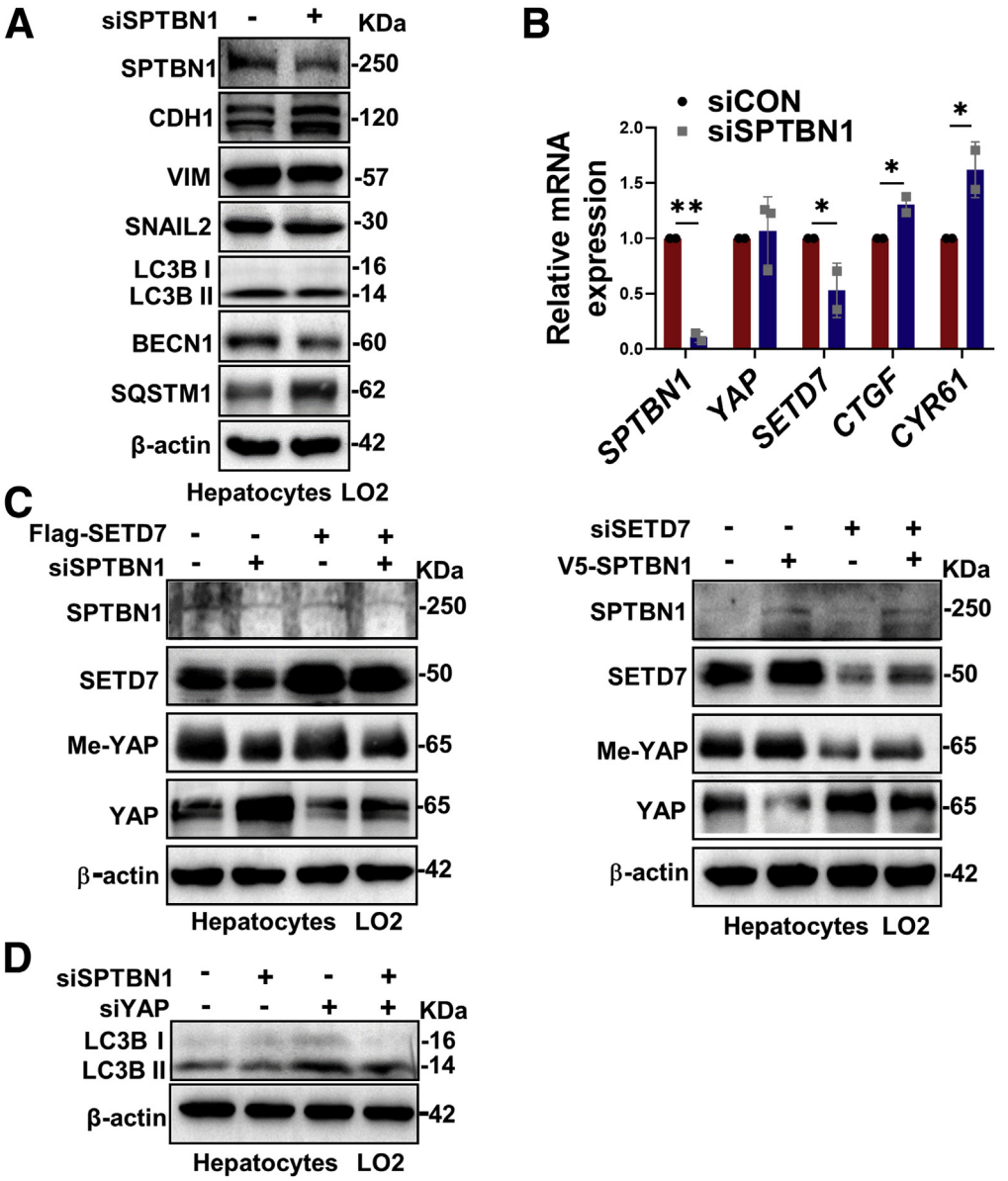

Figure 14. Loss of SPTBN1 inhibited autophagy of normal hepatocyte LO2 by inhibiting YAP methylation. *A*, LO2 were transiently transfected with control siRNA or siRNA to SPTBN1 for 48 hours and then subjected to Western blot analysis. *B*, QRT-PCR. LO2 cells transiently transfected with siRNAs were cultured for 48 hours to detect mRNA levels of *SPTBN1*, *YAP*, *SETD7*, *CYR61*, and *CTGF* (*$P < .05$, **$P < .01$ vs siCON). *C*, Analysis of YAP methylation by Western blot. *Left*, Expression of upregulated YAP and downregulated Me-YAP in LO2 cells with SPTBN1 knockdown was reversed by SETD7 overexpression. *Right*, Expression of downregulated YAP and upregulated Me-YAP in SPTBN1-overexpressing LO2 cells was reversed by SETD7 siRNA. *D*, Western blot. The decreased ratio of LC3BII/LC3B I protein induced by loss of SPTBN1 was reversed by YAP siRNA in LO2 cells.

RFP-LC3 lentivirus purchased from Shanghai Genechem (Shanghai, China). After 24 hours of HBSS-induced autophagy, cells were imaged with an Olympus microscope. The CON-sh- and SPTBN1-sh-transfected Huh-7 and PLC/PRF/5 cells were incubated with HBSS for 24 hours, fixed in 2.5% glutaric dialdehyde solution, and then observed with a transmission electron microscope.

Western Blot and Coimmunoprecipitation

Whole cell extracts were prepared using RIPA buffer. Nuclear and cytoplasmic fractions were separated by a Nuclear and Cytoplasmic Protein Extraction Kit (Beyotime Institute of Biotechnology, Beijing, China). For each sample, an equal amount (40 μg–100 μg) of protein was loaded onto sodium dodecyl sulphate–polyacrylamide gel electrophoresis gels, electrotransferred onto Immobilon-P membranes (Millipore, Bedford, MA), blocked with 5% skim milk in TBST, and incubated with specific primary and the corresponding horseradish peroxidase-conjugated secondary antibodies. Blots were detected using an ECL kit (Catalog#180-501, Tanon, Shanghai, China). Densitometric quantification was performed using ImageJ software.

To detect the methylation of YAP, cell supernatants were incubated with anti-YAP antibody at 4 °C overnight. The immune complexes were recovered with protein G magnetic beads (Bio-Red, Hercules, CA), which were then washed 4 times with lysis buffer; the immunoprecipitants were then subjected to Western blot analysis. Rabbit polyclonal antibody to Methylated Lysine (Anti-Methylated Lysine, Abcam, MA) was used to incubate the blot.

To detect the interaction between proteins, the supernatants of whole cell extracts were incubated with antibodies at 4°C overnight. Immune complexes were subsequently pulled down using protein G magnetic beads (Bio-Red, Hercules, CA). The complexes and whole cell extracts were then analyzed by Western blot analysis. The antibodies used in Western blot and Co-IP are listed in Supplementary Table 4.

Luciferase Assay

To investigate the *SETD7* promoter activity in SPTBN1 knockdown PLC/PRF/5 cells, pGL3-luciferase reporter plasmids comprising the *SETD7* promoter fragment (Supplementary Table 5) were generated using the Hieff Clone Plus One Step Cloning Kit (YEASEN, Shanghai, China). PLC/PRF/5 cells transfected with SPTBN1 siRNA or CON siRNA were assessed using a Dual-Luciferase Reporter Assay System (Promega, Madison, WI) after transfection with SETD7 pGL3-luciferase reporter plasmids or mutants for 24 hours.

Chromatin IP Quantitative PCR

In brief, chromatin fragments derived from PLC/PRF/5 cells were immunoprecipitated with 5 μg of the antibody against SPTBN1, Ig G (3900S, CST, Danvers, MA, USA) or H3 (4620S, CST, Danvers, MA, USA). DNA extraction was purified using a Qiagen Purification kit. Real-time PCR analysis was performed with primers amplifying the promoters of *SETD7* (Forward 5' to 3' AGAATGGACAGGAGCCTTCTAA, Reversed 5' to 3' TATCCCCTGGGGTACATGCT). The antibodies used in the above experiments are listed in Supplementary Table 4.

RNA Extraction and qRT-PCR

Total RNA was extracted from cells using TRIzol-trichloromethane-isopropanol reagent and reverse transcribed into cDNA using the ReverTra Ace qPCR RT Kit (TOYOBO, Osaka, Japan). The 10 μl real-time PCR system contained 10 ng/μl cDNA, 5 μl SYBR Green, 4 μl ddH2O and 1 μl mixed primers. The primer sequences for targeted genes are listed in Supplementary Table 6A and 6B.

Histological Staining

Hematoxylin and eosin (H&E) staining of liver tissues was used to identify liver cancers that developed in *Sptbn1*$^{+/-}$ mice. For immunohistochemistry staining, sections were dewaxed, rehydrated, blocked, incubated with primary antibodies for SPTBN1 (1:300), YAP (1:500), p-YAPS127 (1:600), and SQSTM1 (1:500) and corresponding horseradish peroxidase-conjugated secondary antibodies, and finally incubated with hematoxylin for nuclear staining. Information from patients for the tissue microarray (Ribiology Company, Wuhan, Hubei, China) is presented in Supplementary Table 7. For immunofluorescence staining, after incubation with primary antibodies, sections were incubated with a corresponding fluorescently conjugated secondary antibody. Nuclei were stained with 4'6-diamidino-2-phenylindole.

For immunocytochemistry, cells were fixed in 4% paraformaldehyde for 15 minutes and then permeabilized with 0.1% Triton X-100 for 20 minutes. After blocking with 5% goat serum for 2 hours, cells were incubated with primary antibodies overnight at 4°C. Then, cells were washed and incubated with secondary antibodies and finally incubated with 4'6-diamidino-2-phenylindole for nuclear staining. Epifluorescent images were acquired with an Olympus microscope.

Analysis of The Cancer Genome Atlas Database and Gene Microarrays

The correlation analysis of SPTBN1 and SETD7 was analyzed by Gene Expression Profiling Interactive Analysis (website: http://gepia.cancer-pku.cn/detail.php?clicktag=correlation) using hepatocellular carcinoma clinicopathological data retrieved from The Cancer Genome Atlas database. Overall survival (OS, n = 364) was determined using the K-M method (website: http://kmplot.com/analysis/index.php?p=service&cancer=liver_rnaseq) by retrieving RNA-seq data on hepatocellular carcinoma provided by Menyhart *et al.*[54]

Gene microarrays of EPCAM^{+} HSCs from WT and *Sptbn1*$^{+/-}$ mice and SNU449 cells transfected with SPTBN1 siRNA or control siRNA were performed by Affymetrix, Inc. (Santa Clara, CA). The Kyoto Encyclopedia of Genes and Genomes pathways and differentially expressed genes were analyzed using OmicsBean.

Statistical Analyses

Data are presented as the mean ± standard deviation. The Student *t* test was used for 2-sample comparisons. Immunohistochemical scores were nonnormally distributed and are presented as the median with range, which was analyzed by rank-sum test for comparison. Pearson correlation test was performed on the correlation analysis. All statistical analyses were completed using GraphPad Prism 8.0 software, and $P < .05$ was accepted as statistically significant.

Supplementary Material

Note: To access the supplementary material accompanying this article, visit the online version of Cellular and Molecular Gastroenterology and Hepatology at www.cmghjournal.org, and at http://doi.org/10.1016/j.jcmgh.2021.10.012.

References

1. Chen W, Zheng R, Baade PD, Zhang S, Zeng H, Bray F, Jemal A, Yu XQ, He J. Cancer statistics in China, 2015. CA Cancer J Clin 2016;66:115–132.
2. Bray F, Ferlay J, Soerjomataram I, Siegel RL, Torre LA, Jemal A. Global cancer statistics 2018: GLOBOCAN estimates of incidence and mortality worldwide for 36 cancers in 185 countries. CA Cancer J Clin 2018; 68:394–424.

3. Siegel RL, Miller KD, Jemal A. Cancer statistics, 2020. CA Cancer J Clin 2020;70:7–30.
4. Machnicka B, Czogalla A, Hryniewicz-Jankowska A, Bogusławska DM, Grochowalska R, Heger E, Sikorski AF. Spectrins: a structural platform for stabilization and activation of membrane channels, receptors and transporters. Biochim Biophys Acta 2014; 1838:620–634.
5. Zhang R, Zhang C, Zhao Q, Li D. Spectrin: structure, function and disease. Sci China Life Sci 2013; 56:1076–1085.
6. Abdi KM, Bennett V. Adducin promotes micrometer-scale organization of beta2-spectrin in lateral membranes of bronchial epithelial cells. Mol Biol Cell 2008; 19:536–545.
7. Smith SA, Sturm AC, Curran J, Kline CF, Little SC, Bonilla IM, Long VP, Makara M, Polina I, Hughes LD, Webb TR, Wei Z, Wright P, Voigt N, Bhakta D, Spoonamore KG, Zhang C, Weiss R, Binkley PF, Janssen PM, Kilic A, Higgins RS, Sun M, Ma J, Dobrev D, Zhang M, Carnes CA, Vatta M, Rasband MN, Hund TJ, Mohler PJ. Dysfunction in the βII spectrin–dependent cytoskeleton underlies human arrhythmia. Circulation 2015;131:695–708.
8. Smith SA, Hughes LD, Kline CF, Kempton AN, Dorn LE, Curran J, Makara M, Webb TR, Wright P, Voigt N, Binkley PF, Janssen PM, Kilic A, Carnes CA, Dobrev D, Rasband MN, Hund TJ, Mohler PJ. Dysfunction of the β2-spectrin-based pathway in human heart failure. Am J Physiol Heart Circ Physiol 2016;310:H1583–H1591.
9. Han B, Zhou R, Xia C, Zhuang X. Structural organization of the actin-spectrin–based membrane skeleton in dendrites and soma of neurons. Proc Natl Acad Sci U S A 2017;114:E6678–E6685.
10. Zhou R, Han B, Xia C, Zhuang X. Membrane-associated periodic skeleton is a signaling platform for RTK transactivation in neurons. Science 2019; 365:929–934.
11. Chen J, Yao ZX, Chen JS, Gi YJ, Munoz NM, Kundra S, Herlong HF, Jeong YS, Goltsov A, Ohshiro K, Mistry NA, Zhang J, Su X, Choufani S, Mitra A, Li S, Mishra B, White J, Rashid A, Wang AY, Javle M, Davila M, Michaely P, Weksberg R, Hofstetter WL, Finegold MJ, Shay JW, Machida K, Tsukamoto H, Mishra L. TGF-β/β2-spectrin/CTCF-regulated tumor suppression in human stem cell disorder Beckwith-Wiedemann syndrome. J Clin Invest 2016;126:527–542.
12. Tang Y, Katuri V, Dillner A, Mishra B, Deng CX, Mishra L. Disruption of transforming growth factor-beta signaling in ELF beta-spectrin-deficient mice. Science 2003; 299:574–577.
13. Kikuchi T, Daigo Y, Ishikawa N, Katagiri T, Tsunoda T, Yoshida S, Nakamura Y. Expression profiles of metastatic brain tumor from lung adenocarcinomas on cDNA microarray. Int J Oncol 2006;28:799.
14. Zhi X, Lin L, Yang S, Bhuvaneshwar K, Wang H, Gusev Y, Lee MH, Kallakury B, Shivapurkar N, Cahn K, Tian X, Marshall JL, Byers SW, He AR. βII-Spectrin (SPTBN1) suppresses progression of hepatocellular carcinoma and Wnt signaling by regulation of Wnt inhibitor kallistatin. Hepatology 2015;61:598–612.
15. Baek HJ, Lee YM, Kim TH, Kim JY, Park EJ, Iwabuchi K, Mishra L, Kim SS. Caspase-3/7-mediated cleavage of β2-spectrin is required for acetaminophen-induced liver damage. Int J Biol Sci 2016;12:172–183.
16. Kitisin K, Ganesan N, Tang Y, Jogunoori W, Volpe EA, Kim SS, Katuri V, Kallakury B, Pishvaian M, Albanese C, Mendelson J, Zasloff M, Rashid A, Fishbein T, Evans SR, Sidawy A, Reddy EP, Mishra B, Johnson LB, Shetty K, Mishra L. Disruption of transforming growth factor-β signaling through β-spectrin ELF leads to hepatocellular cancer through cyclin D1 activation. Oncogene 2007; 26:7103–7110.
17. Mitra A, Yan J, Xia X, Zhou S, Chen J, Mishra L, Li S. IL6-mediated inflammatory loop reprograms normal to epithelial-mesenchymal transition(+) metastatic cancer stem cells in preneoplastic liver of transforming growth factor beta-deficient beta2-spectrin(+/-) mice. Hepatology 2017;65:1222–1236.
18. Miyajima A, Tanaka M, Itoh T. Stem/progenitor cells in liver development, homeostasis, regeneration, and reprogramming. Cell Stem Cell 2014;14:561–574.
19. Sia D, Villanueva A, Friedman SL, Llovet JM. Liver cancer cell of origin, molecular class, and effects on patient prognosis. Gastroenterology 2017;152:745–761.
20. Yu S, Wang Y, Jing L, Claret FX, Li Q, Tian T, Liang X, Ruan Z, Jiang L, Yao Y, Nan K, Lv Y, Guo H. Autophagy in the "inflammation-carcinogenesis" pathway of liver and HCC immunotherapy. Cancer Lett 2017;411:82–89.
21. Shen G, Zheng F, Ren D, Du F, Dong Q, Wang Z, Zhao F, Ahmad R, Zhao J. Anlotinib: a novel multi-targeting tyrosine kinase inhibitor in clinical development. J Hematol Oncol 2018;11:120.
22. Ho TT, Warr MR, Adelman ER, Lansinger OM, Flach J, Verovskaya EV, Figueroa ME, Passegué E. Autophagy maintains the metabolism and function of young and old stem cells. Nature 2017;543:205–210.
23. Lee YA, Noon LA, Akat KM, Ybanez MD, Lee T, Berres M, Fujiwara N, Goossens N, Chou H, Parvin-Nejad FP, Khambu B, Kramer EGM, Gordon R, Pfleger C, Germain D, John GR, Campbell KN, Yue Z, Yin X, Cuervo AM, Czaja MJ, Fiel MI, Hoshida Y, Friedman SL. Autophagy is a gatekeeper of hepatic differentiation and carcinogenesis by controlling the degradation of Yap. Nat Commun 2018;9:4962.
24. Li S, Song Y, Quach C, Guo H, Jang G, Maazi H, Zhao S, Sands NA, Liu Q, In GK, Peng D, Yuan W, Machida K, Yu M, Akbari O, Hagiya A, Yang Y, Punj V, Tang L, Liang C. Transcriptional regulation of autophagy-lysosomal function in BRAF-driven melanoma progression and chemoresistance. Nature Commun 2019;10:1693.
25. Zhang S, Chen Q, Liu Q, Li Y, Sun X, Hong L, Ji S, Liu C, Geng J, Zhang W, Lu Z, Yin Z, Zeng Y, Lin K, Wu Q, Li Q, Nakayama K, Nakayama KI, Deng X, Johnson RL, Zhu L, Gao D, Chen L, Zhou D. Hippo signaling suppresses cell ploidy and tumorigenesis through Skp2. Cancer Cell 2017;31:669–684.
26. Meng Z, Moroishi T, Mottier-Pavie V, Plouffe SW, Hansen CG, Hong AW, Park HW, Mo JS, Lu W, Lu S,

Flores F, Yu FX, Halder G, Guan KL. MAP4K family kinases act in parallel to MST1/2 to activate LATS1/2 in the Hippo pathway. Nature Commun 2015;6:8357.
27. Wang P, Gong Y, Guo T, Li M, Fang L, Yin S, Kamran M, Liu Y, Xu J, Xu L, Peng F, Xue X, Yang M, Hung M, Lam EWF, Gu C, Wang C, Zhan Q, Liu Q. Activation of Aurora A kinase increases YAP stability via blockage of autophagy. Cell Death Dis 2019;10:432.
28. Wong KKL, Li W, An Y, Duan Y, Li Z, Kang Y, Yan Y. β-Spectrin regulates the Hippo signaling pathway and modulates the basal actin network. J Biol Chem 2015; 290:6397–6407.
29. Forest E, Logeay R, Géminard C, Kantar D, Frayssinoux F, Heron-Milhavet L, Djiane A. The apical scaffold big bang binds to spectrins and regulates the growth of *Drosophila melanogaster* wing discs. J Cell Biol 2018;217:1047–1062.
30. Fletcher GC, Elbediwy A, Khanal I, Ribeiro PS, Tapon N, Thompson BJ. The Spectrin cytoskeleton regulates the Hippo signalling pathway. EMBO J 2015; 34:940–954.
31. Ma F, Li W, Liu C, Li W, Yu H, Lei B, Ren Y, Li Z, Pang D, Qian C. MiR-23a promotes TGF-beta1-induced EMT and tumor metastasis in breast cancer cells by directly targeting CDH1 and activating Wnt/beta-catenin signaling. Oncotarget 2017;8:69538–69550.
32. Wang Y, Ji T, Nelson AD, Glanowska K, Murphy GG, Jenkins PM, Parent JM. Critical roles of alphaII spectrin in brain development and epileptic encephalopathy. J Clin Invest 2018;128:760–773.
33. Mittal V. Epithelial mesenchymal transition in tumor metastasis. Annu Rev Pathol 2018;13:395–412.
34. Barsyte-Lovejoy D, Li F, Oudhoff MJ, Tatlock JH, Dong A, Zeng H, Wu H, Freeman SA, Schapira M, Senisterra GA, Kuznetsova E, Marcellus R, Allali-Hassani A, Kennedy S, Lambert JP, Couzens AL, Aman A, Gingras AC, Al-Awar R, Fish PV, Gerstenberger BS, Roberts L, Benn CL, Grimley RL, Braam MJS, Rossi FMV, Sudol M, Brown PJ, Bunnage ME, Owen DR, Zaph C, Vedadi M, Arrowsmith CH. (R)-PFI-2 is a potent and selective inhibitor of SETD7 methyltransferase activity in cells. Proc Natl Acad Sci U S A 2014;111:12853–12858.
35. Zhao B, Li L, Tumaneng K, Wang CY, Guan KL. A coordinated phosphorylation by Lats and CK1 regulates YAP stability through SCF -TRCP. Genes Dev 2010; 24:72–85.
36. Hong AW, Meng Z, Yuan HX, Plouffe SW, Moon S, Kim W, Jho EH, Guan KL. Osmotic stress-induced phosphorylation by NLK at Ser128 activates YAP. EMBO Rep 2017;18:72–86.
37. Oudhoff MJ, Antignano F, Chenery AL, Burrows K, Redpath SA, Braam MJ, Perona-Wright G, Zaph C. Intestinal epithelial cell-intrinsic deletion of Setd7 identifies role for developmental pathways in immunity to helminth Infection. PLOS Pathogens 2016;12:e1005876.
38. Oudhoff MJ, Freeman SA, Couzens AL, Antignano F, Kuznetsova E, Min PH, Northrop JP, Lehnertz B, Barsyte-Lovejoy D, Vedadi M, Arrowsmith CH, Nishina H, Gold MR, Rossi FMV, Gingras A, Zaph C. Control of the Hippo pathway by Set7-dependent methylation of Yap. Develop Cell 2013;26:188–194.
39. Cai X, Li H, Kaplan DE. Murine hepatoblast-derived liver tumors resembling human combined hepatocellular-cholangiocarcinoma with stem cell features. Cell Biosci 2020;10:38.
40. Lee KP, Lee JH, Kim TS, Kim TH, Park HD, Byun JS, Kim MC, Jeong WI, Calvisi DF, Kim JM, Lim DS. The Hippo-Salvador pathway restrains hepatic oval cell proliferation, liver size, and liver tumorigenesis. Proc Natl Acad Sci U S A 2010;107:8248–8253.
41. Benhamouche S, Curto M, Saotome I, Gladden AB, Liu CH, Giovannini M, McClatchey AI. Nf2/Merlin controls progenitor homeostasis and tumorigenesis in the liver. Genes Dev 2010;24:1718–1730.
42. Holczbauer A, Factor VM, Andersen JB, Marquardt JU, Kleiner DE, Raggi C, Kitade M, Seo D, Akita H, Durkin ME, Thorgeirsson SS. Modeling pathogenesis of primary liver cancer in lineage-specific mouse cell types. Gastroenterology 2013;145:221–231.
43. Wu JF, Ho MC, Ni YH, Hsu HY, Lee PH, Chang MH. Dysregulation of liver developmental microRNA contribute to hepatic carcinogenesis. J Formos Med Assoc 2020;119:1041–1051.
44. Zhu K, Li J, Li J, Sun J, Guo Y, Tian H, Li L, Zhang C, Shi M, Kong G, Li Z. Ring1 promotes the transformation of hepatic progenitor cells into cancer stem cells through the Wnt/beta-catenin signaling pathway. J Cell Biochem 2019, Online ahead of print.
45. Kim W, Khan SK, Liu Y, Xu R, Park O, He Y, Cha B, Gao B, Yang Y. Hepatic Hippo signaling inhibits protumoural microenvironment to suppress hepatocellular carcinoma. Gut 2018;67:1692–1703.
46. Wang J, Chen Y, Mo PL, Wei YJ, Liu KC, Zhang ZG, Zhang ZW, Chen XP, Zhang L. 1Alpha,25-Dihydroxyvitamin D3 inhibits aflatoxin B1-induced proliferation and dedifferentiation of hepatic progenitor cells by regulating PI3K/Akt and Hippo pathways. J Steroid Biochem Mol Biol 2018;183:228–237.
47. Wilkinson DS, Jariwala JS, Anderson E, Mitra K, Meisenhelder J, Chang JT, Ideker T, Hunter T, Nizet V, Dillin A, Hansen M. Phosphorylation of LC3 by the Hippo kinases STK3/STK4 is essential for autophagy. Mol Cell 2015;57:55–68.
48. Bai ZL, Tay V, Guo SZ, Ren J, Shu MG. Silibinin ;induced human glioblastoma cell apoptosis concomitant with autophagy through simultaneous inhibition of mTOR and YAP. Biomed Res Int 2018;2018:6165192.
49. Liu Z, Zeng W, Wang S, Zhao X, Guo Y, Yu P, Yin X, Liu C, Huang T. A potential role for the Hippo pathway protein, YAP, in controlling proliferation, cell cycle progression, and autophagy in BCPAP and KI thyroid papillary carcinoma cells. Am J Transl Res 2017;9:3212–3223.
50. Yi X, Deng X, Zhao Y, Deng B, Deng J, Fan H, Du Y, Hao L. Ubiquitin-like protein FAT10 promotes osteosarcoma growth by modifying the ubiquitination and degradation of YAP1. Exp Cell Res 2020;387:111804.
51. Liu Y, Deng J. Ubiquitination-deubiquitination in the Hippo signaling pathway (Review). Oncol Rep 2019; 41:1455–1475.

52. Fang L, Teng H, Wang Y, Liao G, Weng L, Li Y, Wang X, Jin J, Jiao C, Chen L, Peng X, Chen J, Yang Y, Fang H, Han D, Li C, Jin X, Zhang S, Liu Z, Liu M, Wei Q, Liao L, Ge X, Zhao B, Zhou D, Qin HL, Zhou J, Wang P. SET1A-mediated mono-methylation at K342 regulates YAP activation by blocking its nuclear export and promotes tumorigenesis. Cancer Cell 2018;34:103–118.
53. Wang Z, Yang X, Chen L, Zhi X, Lu H, Ning Y, Yeong J, Chen S, Yin L, Wang X, Li X. Upregulation of hydroxysteroid sulfotransferase 2B1b promotes hepatic oval cell proliferation by modulating oxysterol-induced LXR activation in a mouse model of liver injury. Arch Toxicol 2017;91:271–287.
54. Menyhart O, Nagy A, Gyorffy B. Determining consistent prognostic biomarkers of overall survival and vascular invasion in hepatocellular carcinoma. R Soc Open Sci 2018;5:181006.

Received February 5, 2021. Accepted October 22, 2021.

Correspondence
Address requests for reprints to: Dr Xiuling Zhi, Department of Physiology and Pathophysiology, School of Basic Medical Sciences, Fudan University, Shanghai, China. e-mail: zhixiuling@fudan.edu.cn; tel: +86-21-54237651; Dr Ping Zhou, Department of Physiology and Pathophysiology, School of Basic Medical Sciences, Fudan University, Shanghai, China. e-mail: zping@shmu.edu.cn; or Dr Aiwu Ruth He, Department of Medicine and Oncology, Lombardi Comprehensive Cancer Center, Georgetown University, Washington, DC. e-mail: arh29@georgetown.edu; tel: +1-202-444-8642; fax:+1-202-542-0435.

Acknowledgment
The authors thank Dr Chen Xu, a pathology doctor from Zhongshan Hospital Affiliated to Fudan University.

CRedit Authorship Contributions
Shuyi Chen (Data curation: Lead; Formal analysis: Lead; Methodology: Lead; Writing – original draft: Lead)
Hujie Wu (Validation: Supporting)
Zhengyang Wang (Methodology: Supporting)
Mengping Jia (Methodology: Supporting)
Jieyu Guo (Formal analysis: Supporting)
Jiayu Jin (Methodology: Supporting)
Xiaobo Li (Methodology: Supporting)
Dan Meng (Project administration: Supporting)
Ling Lin (Methodology: Supporting)
Aiwu Ruth He (Project administration: Equal)
Ping Zhou (Funding acquisition: Equal; Project administration: Equal)
Xiuling Zhi (Funding acquisition: Lead; Project administration: Lead; Writing – review &
editing: Lead)

Conflicts of interest
The authors disclose no conflicts.

Funding
This work was supported by General Programs of the National Natural Science Foundation of China (No.81572713 and No.81874121).

Supplementary Table 1. Differential Expressed Genes for Hippo Pathway, PI3K-Akt/mTOR Pathways (Microarray Analysis of WT vs *Sptbn1*$^{+/-}$ HSCs)

PI3K-Akt signaling pathway	Count = 120	mTOR signaling pathway	Count = 44	Hippo signaling pathway	Count = 44
Gene	Fold change	Gene	Fold change	Gene	Fold change
Pck1	7.588402	*Prkaa2*	3.313512	*Patj*	7.447174
Prlr	6.205024	*Igf1*	2.966077	*Rassf6*	5.249817
Fgfr2	5.559759	*Chuk*	2.715469	*Pard3*	3.618582
Gngt1	5.548901	*Stradb*	2.704452	*Wwc1*	3.548835
Ghr	4.054142	*Irs1*	2.654457	*Bmpr1a*	3.347636
Fgfr4	3.485656	*Rps6kb1*	2.625695	*Fgf1*	2.807672
Sgk2	3.462673	*Prkca*	2.589811	*Pard6b*	2.377636
Creb3l3	3.398698	*Rnf152*	2.41339	*Cdh1*	2.333999
Prkaa2	3.313512	*Cab39l*	2.292622	*Bmp4*	2.257083
Ikbkg	3.115047	*Tbc1d7*	2.244674	*Prkcz*	2.123192
Met	3.068178	*Pten*	2.066916	*Dlg3*	2.115372
Igf1	2.966077	*Mapk3*	−2.06035	*Ywhab*	−2.02804
Bdnf	2.83152	*Rragd*	−2.07648	*Ccnd3*	−2.0925
Fgf1	2.807672	*Flcn*	−2.07943	*Id2*	−2.12387
Chuk	2.715469	*Grb2*	−2.09558	*Ctnna1*	−2.13969
Irs1	2.654457	*Castor2*	−2.16875	*Nkd1*	−2.15902
Rps6kb1	2.625695	*Atp6v1b2*	−2.16939	*Gsk3b*	−2.1746
Prkca	2.589811	*Gsk3b*	−2.1746	*Llgl1*	−2.21941
Gys2	2.574207	*Igf1r*	−2.30931	*Ppp2r2a*	−2.25611
Rbl2	2.570327	*Wdr59*	−2.36484	*Bmp5*	−2.32131
G6pc	2.485964	*Tnfrsf1a*	−2.37198	*Ywhah*	−2.34549
Vtn	2.479085	*Nras*	−2.40049	*Apc*	−2.50835
Fn1	2.43188	*Rps6ka1*	−2.40625	*Serpine1*	−2.53345
Rxra	2.42612	*Akt1*	−2.52956	*Wwtr1*	−2.53556
Vegfa	2.356407	*Rictor*	−2.64083	*Pard6g*	−2.8463
Lamb3	2.197116	*Strada*	−2.76802	*Fzd8*	−2.88065
Them4	2.142961	*Lamtor3*	−2.79703	*Tcf7l1*	−2.97074
Col4a5	2.072375	*Atp6v1h*	−2.82706	*Ccnd1*	−3.07245
Pten	2.066916	*Fzd8*	−2.88065	*Rassf1*	−3.13521
Ywhab	−2.02804	*Rps6ka3*	−2.93579	*Csnk1e*	−3.17693
Itga4	−2.04317	*Pik3r3*	−3.7123	*Lats2*	−3.35052
Creb1	−2.04986	*Castor1*	−3.77316	*Itgb2*	−3.51828
Mapk3	−2.06035	*Fzd6*	−3.94144	*Bmpr2*	−3.52212
Lamb1	−2.06601	*Wnt9b*	−4.09329	*Smad7*	−3.62828
Itgb7	−2.08704	*Slc3a2*	−4.21566	*Tgfbr2*	−3.69774
Thbs2	−2.08887	*Prkcb*	−4.22162	*Fzd6*	−3.94144
Ccnd3	−2.0925	*Pik3cd*	−4.38551	*Wnt9b*	−4.09329
Grb2	−2.09558	*Sgk1*	−4.70343	*Bmp2*	−5.33549
Crtc2	−2.11723	*Grb10*	−5.50352	*Wtip*	−5.54228
Gnb2	−2.12409	*Eif4e*	−5.64502	*Ccnd2*	−5.72462
Lama1	−2.12768	*Akt3*	−6.68715	*Id1*	−6.23852
Pdgfrb	−2.166	*Wnt2*	−8.29182	*Wnt2*	−8.29182
Gsk3b	−2.1746	*Rps6ka2*	−9.14494	*Bmp6*	−8.77418
Jak2	−2.17781	*Tnf*	−9.36789	*Ccn2*	−11.8758

Supplementary Table 1. Continued

PI3K-Akt signaling pathway	Count = 120	mTOR signaling pathway	Count = 44	Hippo signaling pathway	Count = 44
Gene	Fold change	Gene	Fold change	Gene	Fold change
Ppp2r2a	−2.25611				
Sgk3	−2.28178				
Igf1r	−2.30931				
Lama4	−2.32106				
Col4a3	−2.33219				
Ywhah	−2.34549				
Cdk4	−2.37386				
Pik3cg	−2.3803				
Nras	−2.40049				
Lamc1	−2.41417				
Hsp90aa1	−2.45632				
Reln	−2.49724				
Mcl1	−2.52081				
Akt1	−2.52956				
Gnb4	−2.53501				
Gnb1	−2.53936				
Lpar4	−2.56111				
Erbb2	−2.58512				
Ptk2	−2.61244				
Bcl2	−2.66664				
Ppp2r5c	−2.7578				
Col6a3	−2.8139				
Nfkb1	−2.81441				
Col4a4	−2.89443				
Pck2	−2.93795				
Csf1	−2.95712				
Pdgfra	−2.96851				
Pdgfc	−3.01045				
Pik3r5	−3.03443				
Ccnd1	−3.07245				
Lpar6	−3.11387				
Il4r	−3.24021				
F2r	−3.33094				
Itga1	−3.40374				
Csf1r	−3.49223				
Kit	−3.58355				
Bcl2l11	−3.61937				
Pik3r3	−3.7123				
Jak1	−3.74938				
Nr4a1	−3.78545				
Angpt2	−3.79157				
Efna2	−3.83325				
Nos3	−4.00918				
Il3ra	−4.04876				
Tnxb	−4.14256				
Gng2	−4.29327				
Ifnar2	−4.36264				
Pik3cd	−4.38551				

Supplementary Table 1. Continued

PI3K-Akt signaling pathway	Count = 120	mTOR signaling pathway	Count = 44	Hippo signaling pathway	Count = 44
Gene	Fold change	Gene	Fold change	Gene	Fold change
Il6	−4.41769				
Itga6	−4.52203				
Pdgfb	−4.56128				
Pik3r6	−4.68722				
Sgk1	−4.70343				
Ntf3	−4.87067				
Il2rg	−5.10068				
Tlr4	−5.61008				
Eif4e	−5.64502				
Gngt2	−5.67983				
Ccnd2	−5.72462				
Flt1	−5.74386				
Col4a1	−5.80492				
Col4a2	−6.55273				
Akt3	−6.68715				
Itga9	−6.71574				
Flt4	−6.78615				
Tlr2	−7.05292				
Itga5	−7.12998				
Osmr	−7.34988				
Gng11	−8.18049				
Kdr	−8.25627				
Pdgfd	−8.29916				
Lamb2	−10.7514				
Itga8	−11.4952				
Vwf	−12.4518				
Cdkn1a	−12.8695				
Tek	−16.4338				

Supplementary Table 2. Differential Expressed Methylation-related Genes in WT-HSC and *Sptnb1*$^{+/-}$-HSC

Gene	Fold change
Nnmt	5.7
Shmt1	4.5
Anubl1	4.07
Ube2k	4.04
Tpmt	3.8
Ube2u	3.77
Mettl1	3.3
Shmt2	3
Pemt	2.9
Rnmtl1	2.6
Ube2v2	2.58
Ube2l6	2.52
Uba6	2.46
Setd6	2.4
Mettl5	2.3
Usp2	2.27
Uba3	2.26
Usp24	2.22
Setd4	2.2
Setd5	2.1
Ufc1	2.02
Trmt5	2
Comtd1	−2
Uba2	−2.03
Ubap2l	−2.05
G2e3	−2.14
Usp12	−2.17
Arih1	−2.18
Usp7	−2.44
Uhrf2	−2.47
Setd7	−2.5
Dnmt1	−2.9
Usp27x	−3.39
Uba7	−3.48
Dnmt3a	−3.7
Mtr	−3.8
Ubash3b	−3.86
Prmt2	−4.3
Sptbn1	−4.8
Hecw2	−19.47

Supplementary Table 3. The Sequences of siRNAs for Target Genes

Name	Sense (5' to 3')	Antisense (5' to 3')
SPTBN1-1	GGAAUUGCAGAGGACGUCUAGUAUC	GAUACUAGACGUCCUCUGCAAUUCC
SPTBN1-2	ACCUUCGAGAUGGACGGAUGCUCAU	AUGAGCAUCCGUCCAUCUCGAAGGU
NC	GGAACGUGGAGUGCAGAUCUUAAUC	GAUUAAGAUCUGCACUCCACGUUCC
YAP-1	GACAUCUUCUGGUCAGAGATT	UCUCUGACCAGAAGAUGUCTT
YAP-2	ACGUUGACUUAGGAACUUUTT	AAAGUUCCUAAGUCAACGUTT
NC	AACGAUGAUACAUGACACGAG	CUCGUGUCAUGUAUCAUCGUU
SETD7-1	GGGCACCUGGACGAUGACGGAdTdT	UCCGUCAUCGUCCAGGUGCCCdTdT
SETD7-2	GGAGUGUGCUGGAUAUAUUdTdT	AAUAUAUCCAGCACACUCCdTdT
SETD7-3	CAAACUGCAUCUACGAUAUdTdT	AUAUCGUAGAUGCAUUUGdTdT
NC	AACAGCGACUACACCAAUAGA	UCUAUUGGUGUAGUCGCUGUU

Supplementary Table 4. Antibodies Used in Western Blot, IP, and Immunohistochemistry Staining

Antibody	Catalog No.	Company	Country
SPTBN1	SC1180	Genscript	China
Epcam	21050-1-AP	Proteintech	USA
β-actin	66009-1-Ig	Proteintech	USA
EMT antibody sampler kit	9782	CST	USA
CK-19	sc-376126	Santa Cruz	USA
AFP	14550-1-AP	Proteintech	USA
LC3BI/II	3868	CST	USA
Beclin1	3495	CST	USA
SQSTM1/p62	ab56416	Abcam	UK
YAP1	4912/ 66900-1-Ig	CST/ Proteintech	USA
p-YAP^{S127}	4911	CST	USA
LATS1	9157	CST	USA
p-LATS1	9153	CST	USA
ASCL1	ab223229	Abcam	UK
NANOG	sc-134218	Santa Cruz	USA
SETD7	ab124708	Abcam	UK
H3K4 me	5326	CST	USA
H3	ab176842	Abcam	UK
Anti-Methylated Lysine	ab23366	Abcam	UK
V5	sc-271926	Santa Cruz	USA
GFP	sc-53882	Santa Cruz	USA
Flag	F3165	Sigma-Aldrich	USA
Goat anti-Rabbit HRP IgG	A0208	Beyotime	China
Goat anti-Mouse HRP IgG	A0216	Beyotime	China
Alexa Fluor 488-labeled goat anti-mouse IgG (H+L)	A0428	Beyotime	China
Cy3-labeled goat anti-rabbit IgG (H+L)	A0521	Beyotime	China

Supplementary Table 5. Primer Sequences of the Promotor of *SETD7*

Primer	Sequence (5' to 3')
Forward	CGAGCTCTTACGCGTGCTAGCC ACCTCTCGTTGGCCAAAACT
Reversed	CAGTACCGGAATGCCAAGCTTA TGTGCATTCCCCAGCTCATT

Supplementary Table 6A. The Murine Primer Sequences Used in the qRT-PCR Analysis

Gene name	Forward primer (5' to 3')	Reverse primer (5' to 3')
Sptbn1	CGTGAGGACCTACTGGATCAT	GTCCACGTCGTCTTGTGTTTT
Epcam	CGTGAGGACCTACTGGATCAT	GTCCACGTCGTCTTGTGTTTT
Atg4b	TATGATACTCTCCGGTTTGCTGA	GTTCCCCCAATAGCTGGAAAG
Atg5	TGTGCTTCGAGATGTGTGGTT	GTCAAATAGCTGACTCTTGGCAA
Atg7	GTTCGCCCCCTTTAATAGTGC	TGAACTCCAACGTCAAGCGG
Atg10	GTAGTTACCAAGTGCCGGTTC	AGCTAACGGTCTCCCATCTAAA
Becn1	ATGGAGGGGTCTAAGGCGTC	TCCTCTCCTGAGTTAGCCTCT
Snail2	TGGTCAAGAAACATTTCAACGCC	GGTGAGGATCTCTGGTTTTGGTA
Snail	CACACGCTGCCTTGTGTCT	GGTCAGCAAAAGCACGGTT
Vim	CGTCCACACGCACCTACAG	GGGGGATGAGGAATAGAGGCT
Cdh1	CAGGTCTCCTCATGGCTTTGC	CTTCCGAAAAGAAGGCTGTCC
Cdh2	AGCGCAGTCTTACCGAAGG	TCGCTGCTTTCATACTGAACTTT
Cldn1	GGGGACAACATCGTGACCG	AGGAGTCGAAGACTTTGCACT
Ctnnb1	ATGGAGCCGGACAGAAAAGC	CTTGCCACTCAGGGAAGGA
Tjp1	GCCGCTAAGAGCACAGCAA	TCCCCACTCTGAAAATGAGGA
Zeb1	GCTGGCAAGACAACGTGAAAG	GCCTCAGGATAAATGACGGC
Twist1	GGACAAGCTGAGCAAGATTCA	CGGAGAAGGCGTAGCTGAG
Afp	AGCTTCCACGTTAGATTCCTCC	ACAAACTGGGTAAAGGTGATGG
Actin, beta	GGCTGTATTCCCCTCCATCG	CCAGTTGGTAACAATGCCATGT
Pkm	CGCAACACTGGCATCATTT	TGGCTTCACGGACATTCTT
Krt19	GCCGAGAAGAACCGGAAGGATG	CAGCTCCTCAATCCGAGCAAGGT
Thy1	GAACCAAAACCTTCGCCT	GCTCACAAAAGTAGTCGCC
Gja1	CCCATCCAAAGACTGCGG	CGCTGGCTTGCTTGTTGTA
kit	GCCACGTCTCAGCCATCTG	GTCGCCAGCTTCAACTATTAACT
Rplp0	AGATTCGGGATATGCTGTTGGC	TCGGGTCCTAGACCAGTGTTC

Supplementary Table 6B. The Human Primer Sequences Used in the qRT-PCR Analysis

Gene name	Forward primer (5' to 3')	Reverse primer (5' to 3')
SPTBN1	ATCTAACGCACACTACAACCTG	TCAAGCACCTTTCCAATTCGT
ASCL1	CCCAAGCAAGTCAAGCGACA	AAGCCGCTGAAGTTGAGCC
NANOG	TTTGTGGGCCTGAAGAAAACT	AGGGCTGTCCTGAATAAGCAG
BECN1	GGTGTCTCTCGCAGATTCATC	TCAGTCTTCGGCTGAGGTTCT
ATG4B	GGTGTGGACAGATGATCTTTGC	CCAACTCCCATTTGCGCTATC
ATG5	AGAAGCTGTTTCGTCCTGTGG	AGGTGTTTCCAACATTGGCTC
ATG7	ATGATCCCTGTAACTTAGCCCA	CACGGAAGCAAACAACTTCAAC
ATG10	ATAAGATGCGACTGCTACAGGG	CAATGCTCAGCCATGATGTGAT
LAST1	CCACCCTACCCAAAACATCTG	CGCTGCTGATGAGATTTGAGTAC
YAP	TGGGACTCAAAATCCAGTGTC	CCATCTCCTTCCAGTGTTCC
CTGF	AAAAGTGCATCCGTACTCCCA	CCGTCGGTACATACTCCACAG
CYR61	CTCGCCTTAGTCGTCACCC	CGCCGAAGTTGCATTCCAG
SETD7	GGCCAGGGAGTTTACACTTAC	CTCATCAGGGTACACATAGGCTA
ACTIN, beta	CATGTACGTTGCTATCCAGGC	CTCCTTAATGTCACGCACGAT

Supplementary Table 7. Clinical Characteristics of the 24 Patients Used for the Tissue Microarray

Item	Classification	Amount	Item	Classification	Amount
Gender	Male	18	Age, years	>50	10
	Female	6		≤50	14
Maximum diameter of mass, cm	>5	13	Hepatitis B virus infection	Yes	23
	≤5	11		No	1
Intrahepatic metastasis	Yes	7	Cirrhosis	Yes	10
	No	17		No	14
Lymph node metastasis	Yes	0	Extrahepatic metastasis	Yes	1
	No	24		No	23
Differentiation	Low	10			
	Middle	11			
	High	3			